Western Michigan University
ScholarWorks at WMU

Master's Theses

Graduate College

12-2000

Eustasy Determination from Borehole Data, Onshore New Jersey: New Boreholes and New Porosity Estimates

William Alan Van Sickel

Follow this and additional works at: https://scholarworks.wmich.edu/masters_theses

 Part of the Earth Sciences Commons

Recommended Citation

Van Sickel, William Alan, "Eustasy Determination from Borehole Data, Onshore New Jersey: New Boreholes and New Porosity Estimates" (2000). *Master's Theses*. 4420.
https://scholarworks.wmich.edu/masters_theses/4420

This Masters Thesis-Open Access is brought to you for free and open access by the Graduate College at ScholarWorks at WMU. It has been accepted for inclusion in Master's Theses by an authorized administrator of ScholarWorks at WMU. For more information, please contact wmu-scholarworks@wmich.edu.

EUSTASY DETERMINATION FROM BOREHOLE DATA, ONSHORE NEW JERSEY: NEW BOREHOLES AND NEW POROSITY ESTIMATES

by

William Alan Van Sickel

A Thesis
Submitted to the
Faculty of The Graduate College
in partial fulfillment of the
requirements for the
Degree of Master of Science
Department of Geosciences

Western Michigan University
Kalamazoo, Michigan
December 2000

Copyright by
William Alan Van Sickel
2000

ACKNOWLEDGEMENTS

I would like to thank Dr. Michelle Kominz for her guidance, generosity and patience. I also thank the other members of my graduate committee, Dr. William Harrison and Dr. Dave Barnes, for taking time to review my work.

Secondly, I would like to thank those who provided the data necessary in making this thesis possible and those who gave additional feedback. This includes Dr. Kenneth Miller, Dr. Richard Olsson, Dr. Steve Pekar, Ben Cramer, Dr. Jim Browning, Dr. David Nobes, and Lloyd Mullikin.

Lastly, I would like to thank my family for their love and support. I would particularly like to thank my grandfather who couldn't be here with us today, but would surely be proud of my accomplishments.

William Alan Van Sickel

EUSTASY DETERMINATION FROM BOREHOLE DATA, ONSHORE NEW JERSEY: NEW BOREHOLES AND NEW POROSITY ESTIMATES

William Alan Van Sickel, M.S.

Western Michigan University, 2000

Backstripping analysis of detailed stratigraphic data from the Bass River and Ancora boreholes on the New Jersey Coastal Plain (Ocean Drilling Project Leg 174AX) was conducted to test and refine previous eustatic estimates (Kominz et al., 1998) and provide new Upper Cretaceous estimates. Porosity-depth relationships required by the backstripping method were estimated to supplement those from the Cost B-2 well (Rhodehamel, 1977). Sand and mud porosity at shallow depths (<500 m) obtained here are higher than was seen at the Cost B-2 well.

The Bass River and Ancora boreholes targeted older sequences of the Upper Cretaceous to Paleocene. This new data allow for more accurate estimate of the magnitude of long-term sea-level change and provide new information on older (Cretaceous) short-term signals. Eustatic amplitudes varied by as much as 50 m between Cretaceous sequences, suggesting a maximum amplitude of 3rd order sea-level change of about 90 m. Results from Paleocene and younger strata suggest a long-term ($10^8 - 10^7$ y) eustatic fall of ≈ 100 m and superimposed 3rd order (0.5 – 3 m.y.) eustatic changes of less than ≈ 70 m. Sea-level amplitudes and durations were comparable when sequences are represented at multiple boreholes. This suggests that the resultant curves are an approximation of eustasy.

TABLE OF CONTENTS

Table of Contents—continued

LIST OF TABLES

LIST OF FIGURES

List of Figures—continued

CHAPTER I

INTRODUCTION

Eustasy, or global sea-level change, is a crucial component for understanding earth's history. It is an indicator of glacial and orogenic events and it reveals changes in ocean basin development. Eustasy has been an important subject in the geologic community and continues to be as new data is acquired.

Eustatic events signal their occurrence through the synchronous creation or loss of worldwide accommodation or the space made available for sediment accumulation (Jervey, 1988; Posamentier et al., 1988). The evidence for eustatic events consists of synchronous sedimentary sequences and the unconformities that bound them (Vail, 1988). An eustatic signal is recognized only if it is large enough and is of worldwide extent (Kendall et al., 1992).

The stratigraphic signature in the rock record is a result of the interaction of tectonics and eustasy, both of which control accommodation space (Emery and Myers, 1996). It is difficult to isolate an eustatic signal from a complex regime of controls on sedimentation including tectonic subsidence, sediment compaction, sedimentation rates, thermal cooling rates, etc. Numerous methods of estimating eustasy have been used, but few have isolated an eustatic signal. The backstripping method, originally developed by Sleep (1971), is a quantitative method of estimating tectonic subsidence. Tectonic subsidence is the basement response to tectonic forces under water

and in the absence of sediment. By quantitatively removing the effects of sediment loading and compaction, an approximation of the subsidence that would have occurred if the basin had subsided in water and without sediment deposition can be calculated (Bond and Kominz, 1991). This step is known as the first reduction (R1) and is the basis for identifying the tectonic component of subsidence and comparing it with geodynamic subsidence models in order to extract the eustatic component, known as R2 (Bond et al., 1989).

Geologic Setting

The New Jersey Coastal Plain, located on a stable, mature, passive margin, is an ideal location for estimating eustasy through the backstripping method. Most of the subsidence observed on the coastal plain is due to loading by sediment offshore (Steckler et al., 1988). Therefore, the form of subsidence is that of a thermally subsiding basin in which theoretical subsidence is assumed to be that of a cooling plate (e.g., McKenzie, 1978).

The New Jersey Coastal Plain forms the western margin of the Baltimore Canyon Trough (Figure 1), a large sedimentary basin that underlies the continental shelf along the Middle Atlantic States (Grow and Sheridan, 1988). The New Jersey Coastal Plain formed following Triassic-Early Jurassic rifting between North America and Africa (Grow and Sheridan, 1988). The coastal plain did not form until the Cretaceous when the crust attained sufficient flexural rigidity for offshore thermal subsidence creating accommodation space onshore (Watts, 1981). It consists of Lower Cretaceous

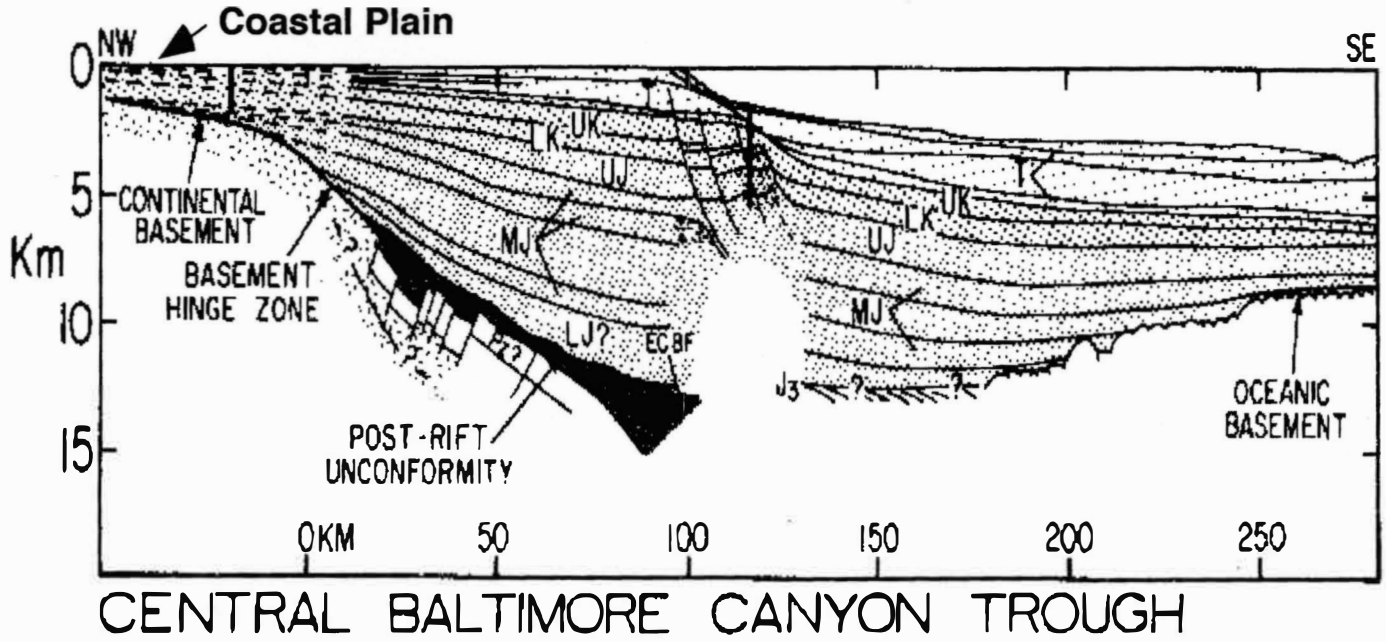

Figure 1. Cross Section of Central Baltimore Canyon Trough. Ages of sedimentary units are T = Tertiary, UK = Upper Cretaceous, LK = Lower Cretaceous, UJ = Upper Jurassic, MJ = Middle Jurassic, LJ = Lower Jurassic.

Source: Adapted from Klitgord et al. (1988, Fig.3B).

to Holocene strata that dip gently (<1°) seaward and thickens down-dip toward the Baltimore Canyon Trough (Miller, 1997). The sediments are primarily unconsolidated siliciclastic sands and muds that were deposited in fluvial to shelfal environments, with a strong deltaic influence in the Cretaceous (Owens and Sohl, 1969; Owens and Gohn, 1985).

The Paleocene and Eocene strata are dominated by clay-rich sediments containing abundant glauconite and carbonate components that were deposited in sediment starved, deep water environments. The Oligocene strata are dominated by sand-rich siliciclastics deposited in a more shoaling environment. Deposition of siliciclastic sands and muds then followed in the Miocene-Holocene in fluvial to shelfal environments (Owens and Sohl, 1969; Owens and Gohn, 1985).

Sedimentation by fluvial processes began on the coastal plain during the Early Cretaceous (Olsson et al., 1988). A major cycle of sea level rise occurred during Mid-Cretaceous leading to the spread of seas over the current coastal plain during the Late Cretaceous where inner-shelf deposits were laid down at the present Atlantic Coastal Plain (Olsson et al., 1988). Fine-grained clastic and carbonate deposits accumulated farther offshore. The Oligocene-Early Miocene witnessed active progradation of the shelf edge. This major pulse of sedimentation occurred when uplift of the Appalachians and climatic cooling led to a tenfold increase in the rate of siliciclastic sediment input to the margin (Poag and Sevon, 1989; Poag, 1992). Sediment was carried to the Northern Baltimore Trough creating a series of deltaic deposits across the shelf (Grow et al., 1988). A general regression occurred

over the last 50 million years. As a result, upper Miocene through Holocene strata are primarily marginal marine to non-marine (Miller, 1997).

The ODP-New Jersey Coastal Plain Drilling Project

A major scientific study, the New Jersey Coastal Plain Drilling Project, is an ODP (Ocean Drilling Project) onshore drilling program intended to identify, date, and map depositional sequences along the New Jersey margin. This project is funded by the National Science Foundation, the New Jersey Geological Survey, and the Delaware Geological Survey. It is a collaborative effort by Rutgers University, Lamont-Doherty Earth Observatory, the New Jersey Geological Survey, the Delaware Geological Survey, the United States Geological Survey, Texas A&M University, Pennsylvania State University, University of California (San Diego), University of Maine (Orono), State University of New York (New Paltz), University of North Carolina (Chapel Hill), Laboratoire de Geologie du Quaternaire (France), Woods Hole Oceanographic Institution, Institute des Sciences de l' evolution (Universite Montpellier II), and the National Institute of Marine Geology and Geoecology (Romania) (Miller et al., 1994; Miller et al., 1998; Miller et al., 1999).

Drilling of boreholes both on and offshore has proven to be essential in obtaining detailed stratigraphic data necessary for understanding the history of sea-level change. A total of seven boreholes have been drilled as part of the New Jersey Coastal Plain Drilling Project (Figure 2). Onshore drilling of ODP Leg 150X included completed boreholes at Island Beach (April-May 1993), Atlantic City (June-August 1993), and Cape May (March-April 1994).

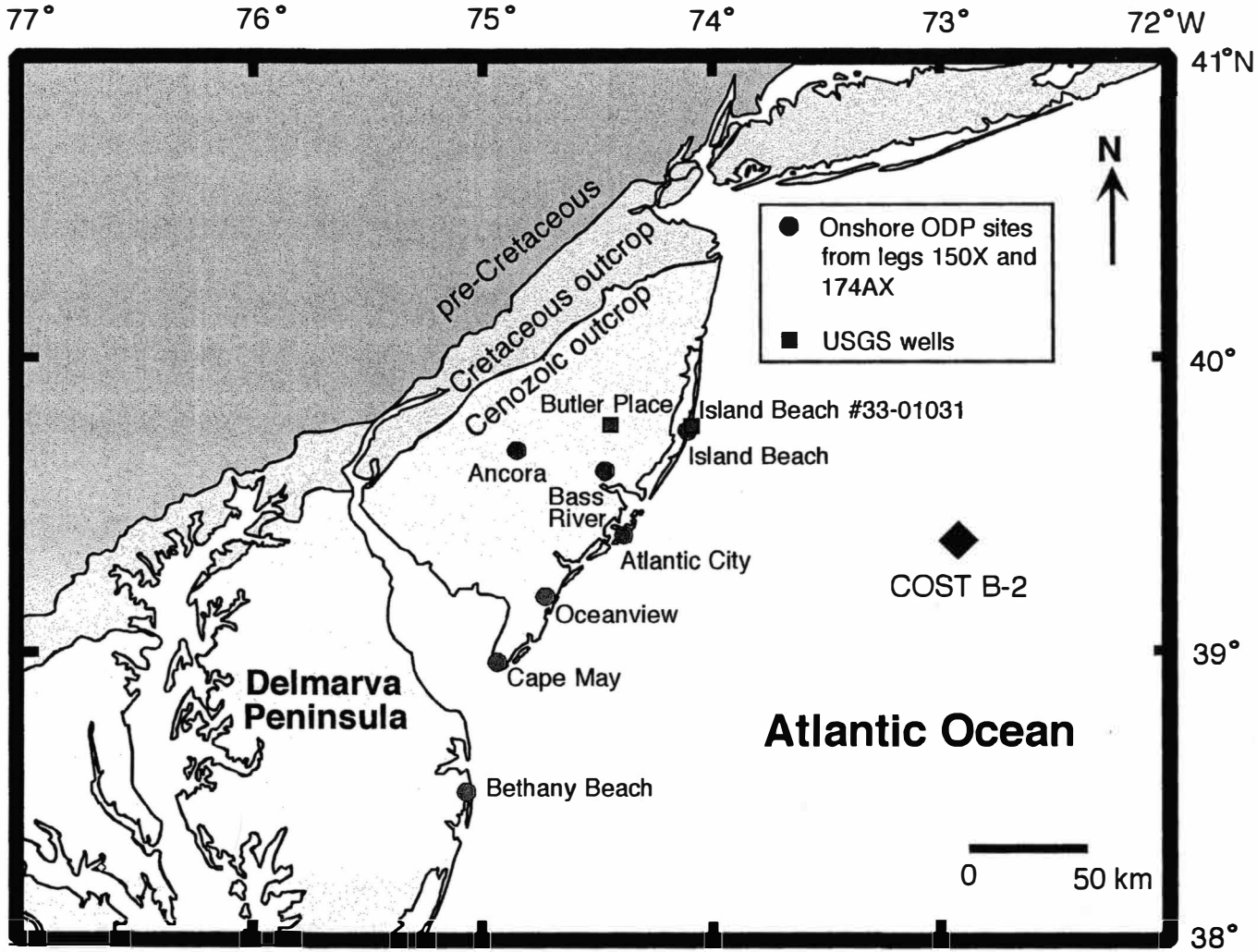

Figure 2. Map Showing Location of New Jersey Coastal Plain Boreholes and Wells Used or Referred to in This Study.

Onshore drilling of ODP Leg 174AX included completed boreholes at Bass River (October-November 1996), Ancora (July-August 1998), Oceanview (September-October 1999), and Bethany Beach (May-June 2000).

Previous Work

One-dimensional analysis, or backstripping, of the first three continuously cored boreholes (Island Beach, Atlantic City, and Cape May) by Kominz et al. (1998) was accomplished using first (R1) and second (R2) reduction curves from detailed stratigraphic data. Comparison of the R2 results revealed that the amplitudes of the R2 curves are similar when sequences are represented in all three boreholes suggesting it was an eustatic signal (Kominz et al., 1998). That is, consistent magnitudes and duration of R2 at different borehole sites are indicators of eustatic change. The R2 results revealed both long-term (10^8–10^7 years) eustatic fall of approximately 100 meters since early Eocene and short-term (0.5-3 m.y.) eustatic falls of less than 70 meters (Kominz et al., 1998). The magnitudes were similar to Kominz's (1984) long-term sea-level estimates and were much lower than those of Haq et al. (1987), although the general trends were similar (Kominz et al., 1998). Short-term (3^{rd} order) sea-level estimates, indicated by the R2 results, were also considerably lower than those of Haq et al. (1987).

This Work

Backstripping analysis of stratigraphic data from the Bass River and Ancora boreholes was conducted to test and refine previous analysis (Kominz

et al., 1998) while providing new eustatic estimates from Upper Cretaceous borehole data. Because these wells are located in a more up-dip direction, they targeted much older sequences. Thus, a primary focus of this new project was upper Cretaceous to Paleocene strata that previously were poorly sampled (Miller et al., 1998). This additional stratigraphic data from early Cenozoic strata was necessary to compare with results from the Island Beach borehole (Kominz et al., 1998). The analyses of the Cretaceous portion of the record should provide a better estimate of the magnitude of long-term sea-level change while it will also yield important information on older short-term eustatic signals (Kominz et al., 1998).

The backstripping method requires detailed stratigraphic data including ages of sequences, paleowater depth estimates, and porosity-depth relationships. Porosity data is used for the decompaction of sedimentary units. Sedimentary units are decompacted in order to remove the effects of sediment loading and compaction on basement subsidence. Therefore, new porosity data from additional sites (Island Beach borehole, Island Beach well #33-01031, and Butler Place well) were quantitatively estimated as part of this research. This new data defined the porosity-depth relationships for this database and replaced those from the poorly sampled Cost B-2 well used by Kominz et al. (1998).

CHAPTER II

POROSITY – DEPTH ANALYSIS

Introduction

Porosity-depth relationships are required to obtain estimates of the magnitude of eustasy using the backstripping method. Because porosity-depth relationships of sediments on the New Jersey Coastal Plain have not been established, new estimates of porosity were calculated.

The previous study of eustasy from boreholes along the New Jersey margin by Kominz et al. (1998) adapted sand (Rhodehamel, 1977) and mud porosity curves from the Cost B-2 well. Because of its distal location and poor sampling at shallow depths, porosity curves from the offshore Cost B-2 well may not be appropriate for the onshore boreholes on the New Jersey Coastal Plain (Figure 2). In this chapter, sand and mud porosity from onshore sites were determined to more accurately define porosity-depth relationships used in this study.

Three wells were chosen for analysis because of the availability of electric logs, lithologic descriptions, and the drilling depth. These wells included the Island Beach borehole (ODP Leg 150X), Island Beach well #33-01031, and Butler Place well (Figure 2). Gamma logs of borehole stratigraphy were used to quantitatively identify sand and mud intervals. Sand was assumed have less than 5% clay by volume and mud as having more than

50% clay by volume. Porosity for these intervals was calculated from sonic logs.

Description of Wells/Boreholes

Island Beach Borehole

The Island Beach borehole (Figure 2) was the first site drilled as part of the New Jersey Coastal Plain Drilling Project Leg 150X. Drilling began in March 1993 at Coast Guard Station 112, Island Beach State Park, New Jersey (39°48'10"N, 74°05'37"; elevation 3.66 m) (Miller et al., 1994). This site recovered Paleocene to Holocene sequences to a total depth of 372.8 m (Miller et al., 1994). Both gamma and sonic logs (Appendix A; Figure 27) were acquired along with onsite core descriptions and grain size analyses. This borehole was selected due to completeness of cores and availability of electric logs.

Island Beach Well #33-01031

The Island Beach well #33-01031 (Figure 2) was an exploratory borehole drilled in 1962 at Island Beach State Park, New Jersey (39°48'29"N, 74°05'35"W; elevation 2.74 m) (Gill et al., 1963). Drilling was undertaken by the U.S. Geological Survey in cooperation with the New Jersey Department of Conservation and Economic Development, Division of Water Policy and Supply (Gill et al., 1963). The Island Beach well #33-01031 was drilled as part of the Water Supply Act of 1958 in order to provide geologic and hydrologic

information for groundwater resource evaluation of southern New Jersey (Gillet al., 1963). Drilling persisted through the entire coastal plain sequence to a total depth of 1,186 m and encountered bedrock at 1,155.5 m. Gamma logs, sonic logs (Appendix A; Figure 28) and core descriptions were acquired onsite. This well was analyzed in order to add data for the interval below the bottom of the Island Bach borehole.

Butler Place Well

The Butler Place well (Figure 2) was an observation well drilled in 1964 at Lebanon State Forest, New Jersey (39°51'22"N, 74°30'17"W; elevation 41.45 m). The well was drilled to a total depth of 700.1 m by the U.S. Geological Survey. Both gamma and sonic logs (Appendix A; Figure 29) were taken along with core descriptions. This well was analyzed to further establish porosity at depths below the Island Beach borehole.

Clay Fraction Analysis

Due to the limited sampling of cores/ cuttings for these wells, with the exception of the Island Beach borehole, clay fraction analysis from gamma logs was used to quantitatively define sand and mud. Sand is abundant in these wells so it was defined as having less than 5% clay by volume. Mud includes both clay and silt-sized grains. In this study, material having more than 50% clay volume was defined as mud. Sand and mud porosities were calculated for those samples that met these criteria. Units not among these criteria were ignored.

Gamma ray logs measure the natural radioactivity given off by different types of radioactive elements within formations including thorium, potassium and uranium. In general, clay-free sands and carbonates have low concentrations of radioactive material characterized by a low gamma response. Gamma ray log responses tend to increase as clay content increases due to the presence of radioactive elements within clays, predominately from potassium. Because clay is more radioactive than sand or carbonate, gamma ray logs are used to calculate the clay fraction in porous materials (Asquith and Gibson, 1982). The following equation (Schlumberger, 1974) was used to determine relative clay fraction of porous sediments.

$$V_{clay} = \left(\frac{GR_{log} - GR_{min}}{GR_{max} - GR_{min}} \right)$$

Where

V_{clay} = clay fraction

GR_{log} = gamma reading of formation

GR_{min} = minimum gamma reading (clean sand)

GR_{max} = maximum gamma reading (100% clay) (1)

A common gamma ray minimum and maximum were arbitrarily chosen to approximate the limits of gamma log responses. A gamma ray minimum of 0 API was used to define pure silica sand while a gamma ray maximum of 250 API was used to define pure clay. Clay fraction ranged from near zero to 100%, but generally was less than 40% (Figure 3). Clay fraction results are consistent with the available well log descriptions, especially with the more

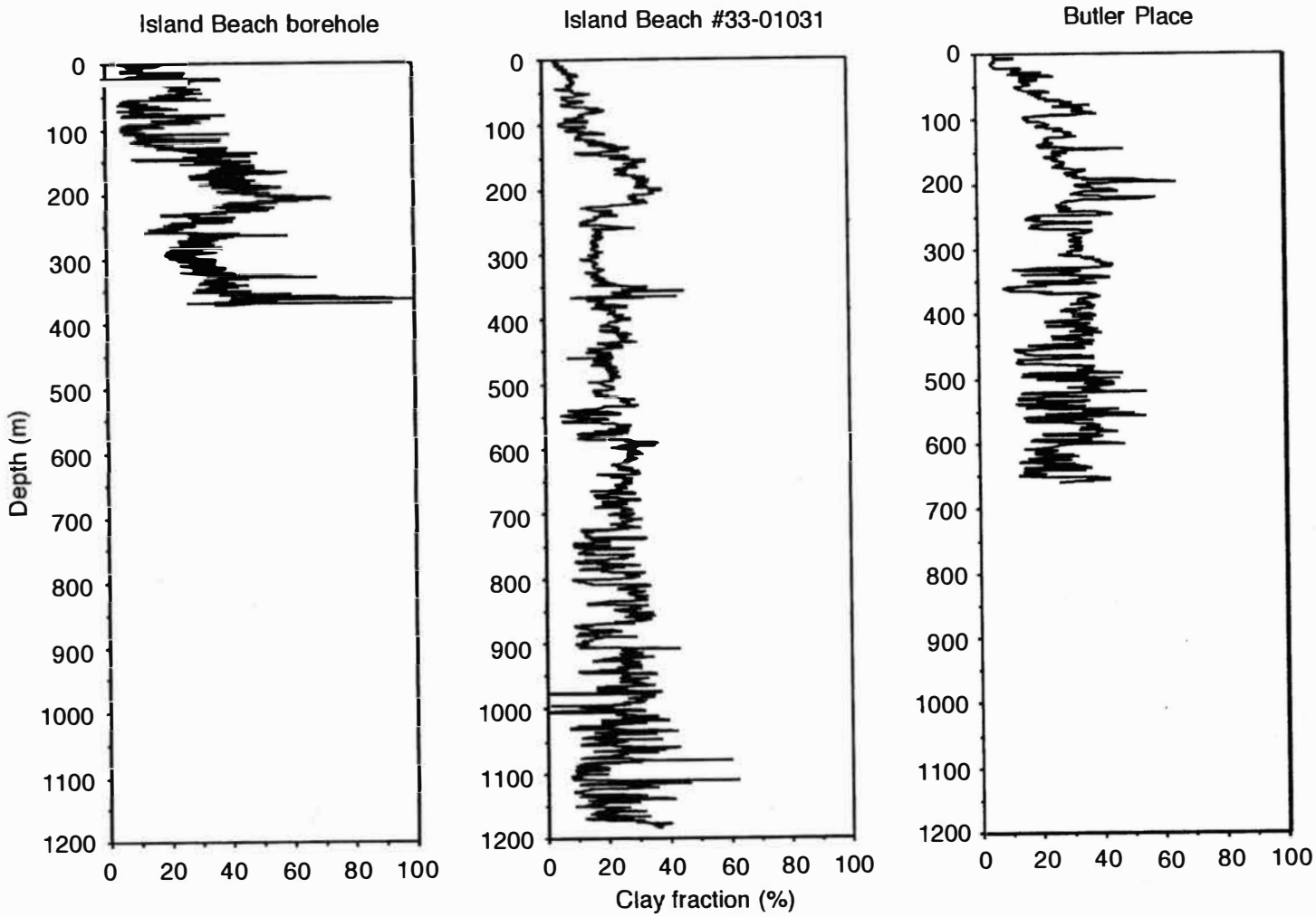

Figure 3. Clay Fraction of the Three Wells Estimated From Gamma Ray Logs.

detailed lithologic descriptions of the Island Beach borehole.

Sonic Porosity Analysis

The sonic log is a porosity log that measures interval transit time (Δt) of a compressional sound wave travelling through the formation (Asquith and Gibson, 1982). Interval transit-time, measured in microseconds per foot, is the reciprocal of the velocity of a compressional sound wave. Theoretically, the travel time of an acoustic signal through the formation is the sum of the travel time through the volumetric percentage of pore space filled by fluid plus the travel time of volumetric percentage of the matrix (Anselmetti and Eberli, 1999). Thus, there is a strong correlation between porosity and velocity. This, however, does not imply that porosity has a direct relationship with velocity. There are physical influences of porosity on dynamic moduli that affect velocity (Gassman, 1951).

Lithostatic pressure is a physical factor that affects velocity. Burial depth is generally a primary factor in determining mechanical compaction because lithostatic pressure increases with depth (Erickson and Jarrard, 1998) (Figure 4). Lithostatic pressure increases framework stiffness by increasing the number and area on intergrain contacts in deeper sediments (Stoll, 1989). Thus, porosity generally decreases as burial depth increases.

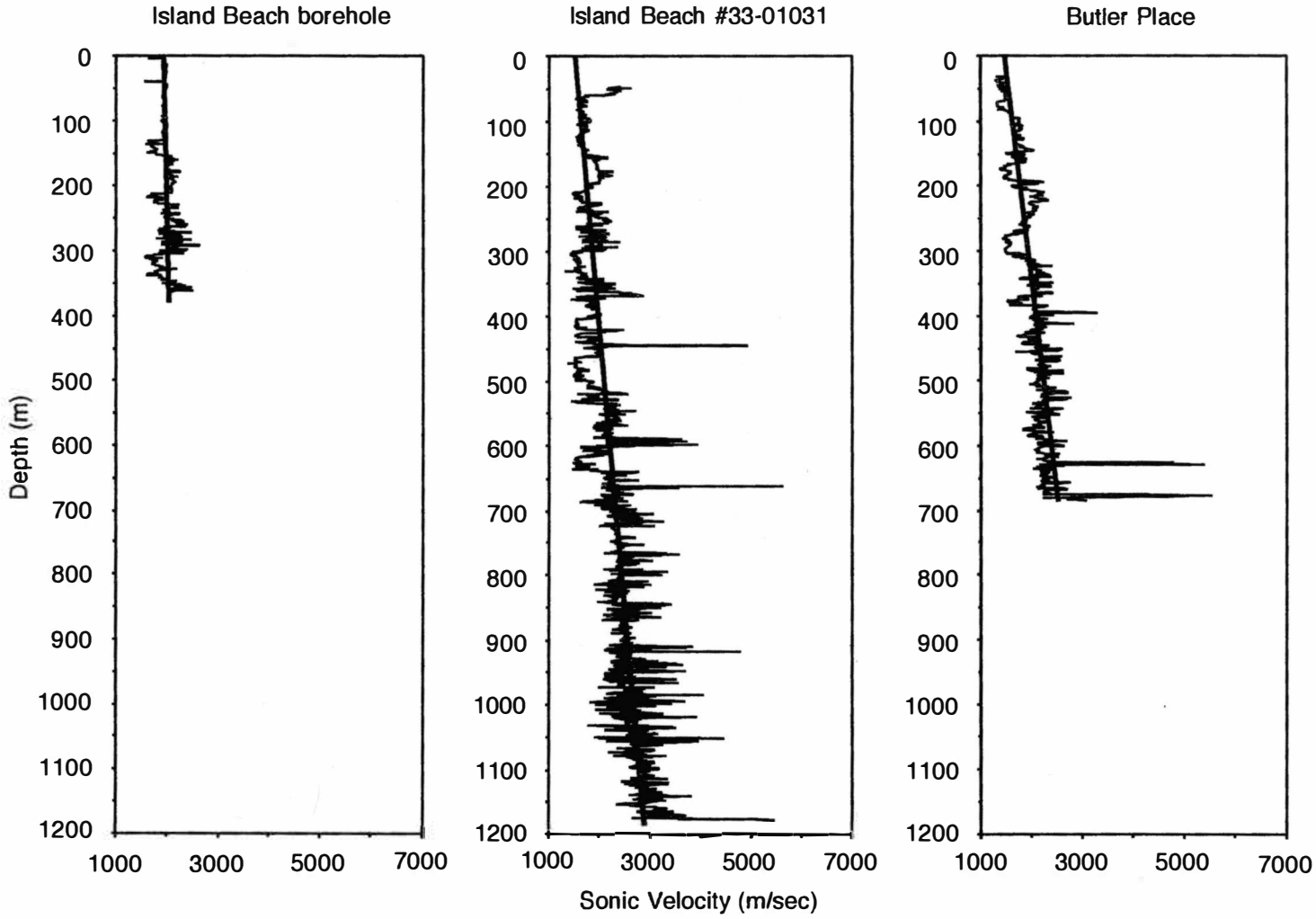

Figure 4. Sonic Velocity of the Three Wells. The trend lines shows the increase of sonic velocity with depth.

Source: The Island Beach borehole data from Miller et al. (1994). The Island Beach #33-01031 and Butler Place well provided by Lloyd Mullikin of the New Jersey Geological Survey.

Table 1

Sonic Velocities and Interval Transit Times for Different Matricies

Matricies	V_{ma} (m/sec)	Δt_{ma} (μsec/m)	Δt_{ma} (μsec/m) commonly used
Sandstone	5,486 to 5,944	182 to 168	182 to 168
Limestone	6,400 to 7,010	156 to 143	156
Dolomite	7,010 to 7,925	143 to 126	143
Anhydrite	6,096	164	164
Salt	4,572	219	219
Mud	3,400 to 4,500	294 to 222	294 to 222
*Water	1,500	667	667

Source: Modified from Schlumberger (1972). *Data from Anselmetti and Eberli (1999).

Sonic velocity is also dependent on lithology (Table 1). Sediments of the New Jersey Coastal Plain are dominated by a combination of sand and clay where most lithologic variations are related to clay content. Clay, having a sonic velocity of 3,400 m/sec, can significantly decrease sonic velocity of a formation. Pure silica sand has a sonic velocity around 6,000 m/sec. Mud is heterogenous in composition and therefore also in matrix velocity (Erickson and Jarrard, 1998). Variations in clay fraction can make it difficult to determine a matrix velocity for mud (e.g., Table 2).

Table 2

Sonic Velocities and Interval Transit Times for a Mud Matrix

Matrix	V (m/sec)	Δt (μsec/m)	Source
mud	4,500	222	Schlumberger (1989), Magara (1976)
mud	4,300	233	Erickson and Jarrard (1998)
Mud with 70% clay	4,000	250	Nobes et al. (1992)
100 % clay	3,400	294	Nobes et al. (1991)

The following equation (Wyllie et al., 1958) is used here to determine sonic derived porosity of the formation.

$$\phi_{sonic} = \left(\frac{\Delta t_{\log} - \Delta t_{ma}}{\Delta t_f - \Delta t_{ma}} \right)$$

Where

ϕ_{sonic} = sonic derived porosity

Δt_{ma} = interval transit time of the matrix

Δt_{log} = interval transit time of formation

Δt_f = interval transit time of the fluid in the well bore (2)

For this study, 233 μsec/m (Erickson and Jarrard, 1998) was chosen for the travel time of mud, 168 μsec/m (Schlumberger, 1972) for sand, and 667 μsec/m (Anselmetti and Eberli, 1999) for pore fluid (fresh water).

Sand and Mud Porosity-Depth Results

Sand and mud porosity in the upper 400 meters are well represented by the Island Beach borehole while the Island Beach well #33-01031 defines porosity below 900 m (Figure 5). Sand porosity near the surface is approximately 70% and decreases to about 40% to 60% at a depth of a kilometer. Mud porosity at 200 meters depth ranges between 50% and 80% and decreases to about 20% to 40% at 1,100 meters depth.

The porosity results from the three wells were combined to approximate the relationship of porosity with depth for sand and mud on the New Jersey Coastal Plain (Figure 6). Because these porosity results ranged from the surface to basement depths, they are crucial in defining the compaction rates of sediments in this region. This is extremely important when applying the backstripping method to borehole stratigraphy from the New Jersey Coastal Plain.

Discussion

Results from Figure 6 are added to the Cost B-2 well porosity data to more accurately define sand and mud porosity in the upper kilometer and to include deeper porosity estimates (Figure 7). This figure illustrates the upper and lower limits for sand and mud porosity-depth relations used by Kominz et al. (1998). The previous porosity data used by Kominz et al. (1998) are high to other analysis for sand and mud. The average porosity for sand near surface depths range from 20% to 45% (e.g. Magara, 1980). Shales have an

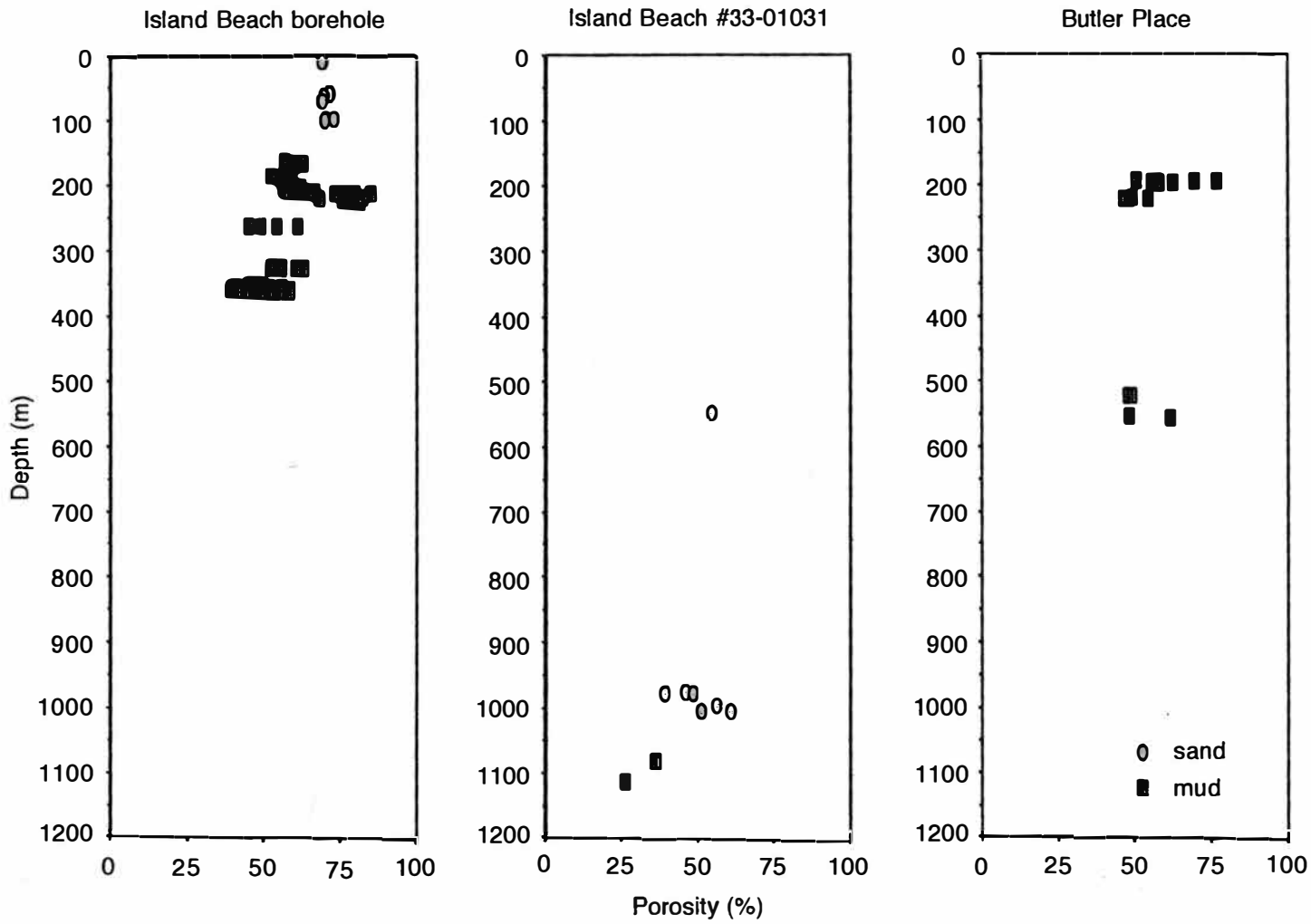

Figure 5. Sonic Derived Sand and Mud Porosity for the Three Wells.

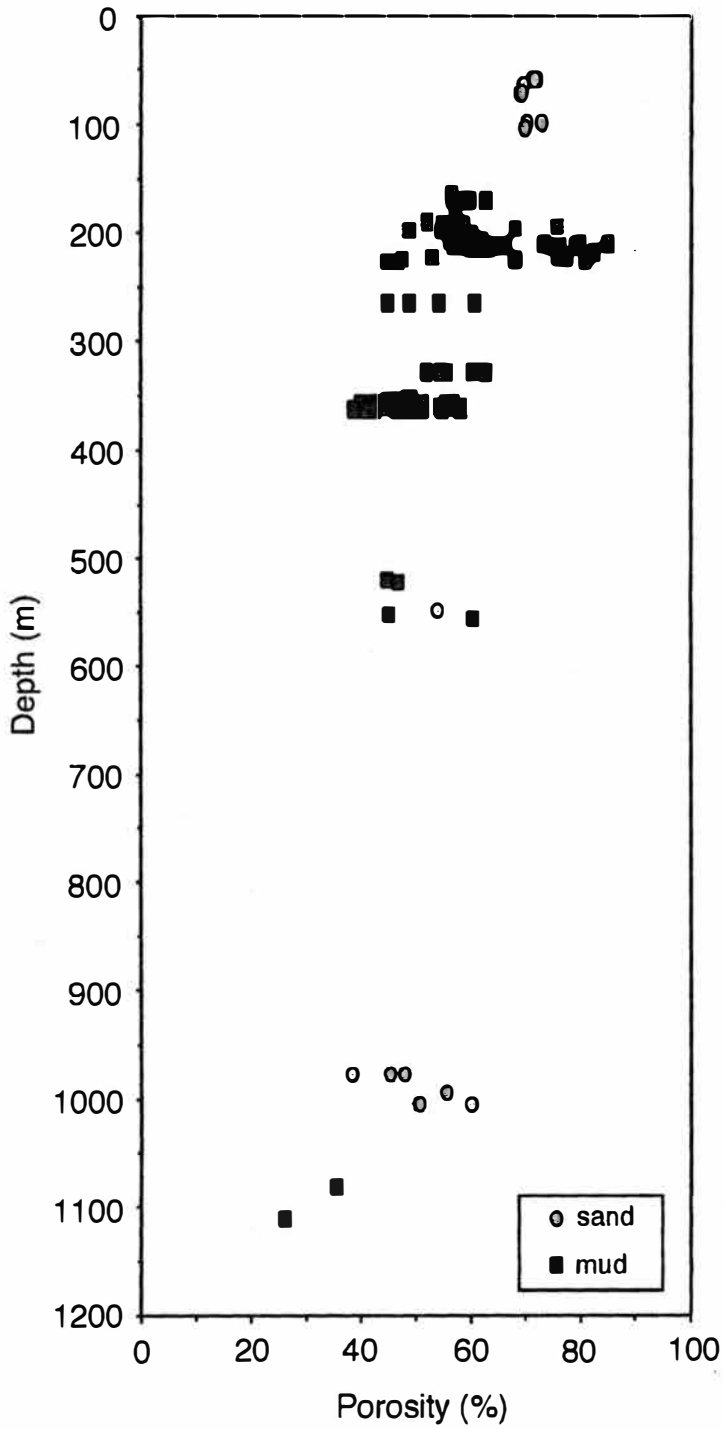

Figure 6. Porosity-Depth Relationship for Sand and Mud.

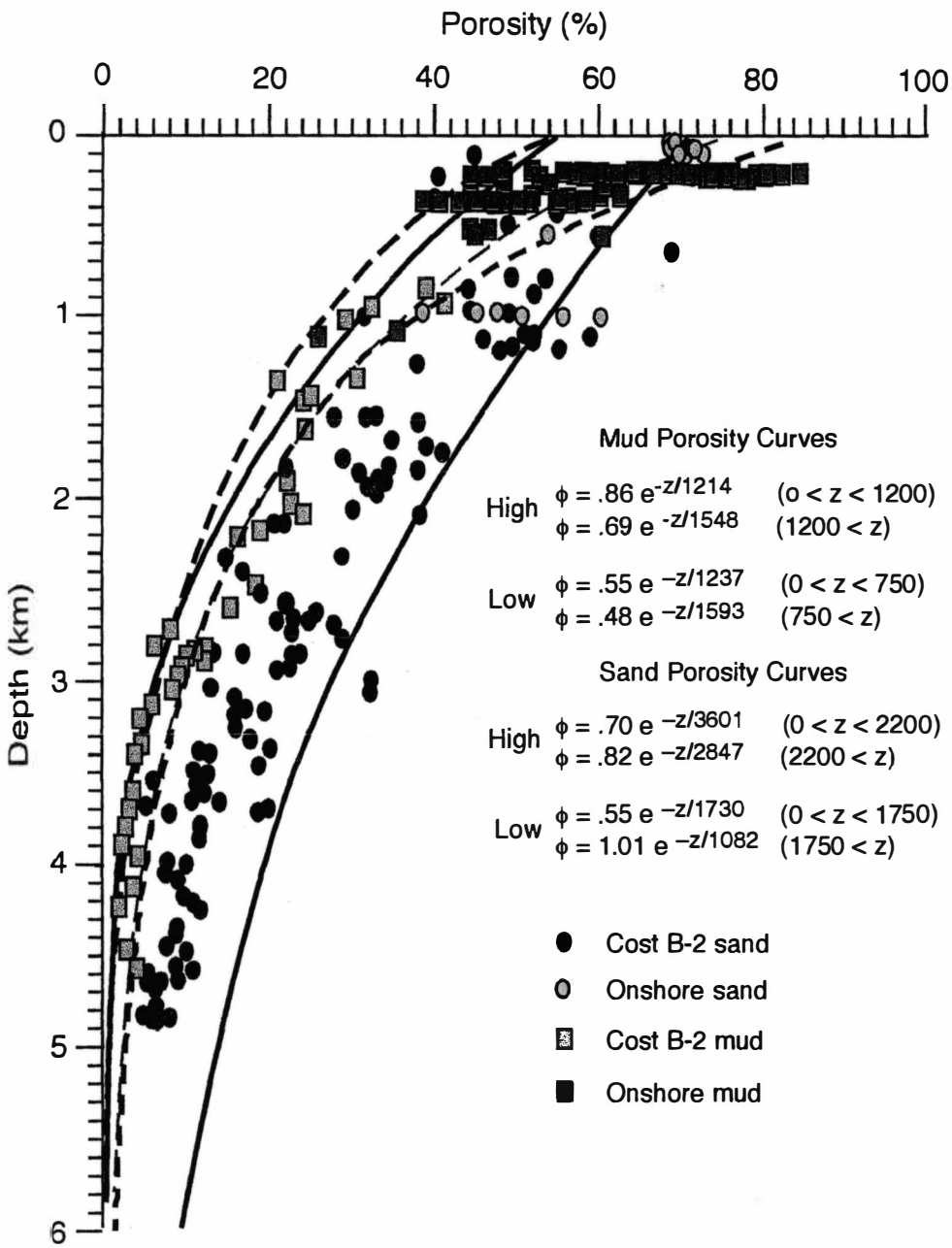

Figure 7. Cost B-2 Sand and Mud Porosity With New Porosity Estimates From Island Beach Borehole, Island Beach Well #33-01031, and Butler Place Well.

Source: Modified from Kominz and Pekar (2000).

average porosity from 30% to 70% near the surface (e.g. Magara, 1980). Since no real porosity analyses have been done on mud, porosity results from shale are used for comparison.

Although porosity results are high to other documented sources, they are quite consistent to the Cost B-2 well analysis (Rhodehamel, 1977) used by Kominz et al. (1998). The new porosity data clearly requires higher porosity in the upper limits of mud when compared to the original curves. The upper limit for mud porosity increased from 75% to 86% at zero depth. This produces a wider range of mud porosity from 55% to 86% at the surface. Sand porosity remains equivalent to previous results.

The porosity of mud in the shallow subsurface is greater than that of sand, but mud porosity decreases at a greater rate as a function of depth. This observation can simply be explained by the grain texture of these sediments and their response to increase in pressure (Figure 8). Sand-rich sediments compact at a relatively constant rate before chemical compaction takes place (Magara, 1980). Chemical compaction of sand usually occurs when the porosity decreases to 20% to 25%, the depth of closest packing (Velde, 1996). On the other hand, muddy sediments have an initial high porosity due to the plate-like shape of clay minerals allowing removal of significant pore fluid with burial (Magara, 1980). Muddy sediments contain silt to clay-sized grains of clay and with contrasting shapes. The clay particles arrange themselves into a sponge-like structure where the plates are attached or attracted edge to edge (Meade, 1964). This process, known as flocculation, occurs due to the charged edges of these plates where the crystal structure is

incomplete. When compacted, these clay particles begin to align themselves parallel to one another such that porosity decreases at a rapid rate. Dewatering and chemical compaction begin to occur once the mineral grains are aligned. Subsequently, beneath this depth, porosity decreases at a much slower rate.

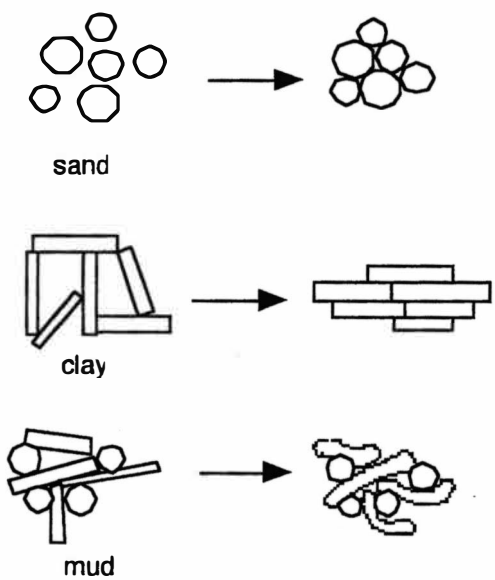

Figure 8. Schematic Representation of the Textural Pattern of Grains for Sand and Mud as a Result of Compaction.

When the plate-like shape of clay minerals and the spherical shape of silica minerals are combined, as is the case for muddy sediments, the initial void ratio at shallow depths are quite high. With increased pressure, the clay particles begin to conform around the external surface of the silica grains due to the ductile nature of clay minerals. Therefore, mud porosity decreases more rapidly with depth than sand. Once the clay minerals have conformed

around the silica grains, dewatering and chemical compaction begin to take place. Porosity then decreases at a much slower rate as a function of depth.

Empirical porosity-depth curves were used to quantitatively decompact borehole stratigraphy for the Bass River and Ancora boreholes (Figure 9). The assumption is made that the ranges between the limits contain the correct values for decompaction. Sand and mud porosities include new estimates (Figure 7) with the Cost B-2 well porosities (Rhodehamel, 1977). The new estimates of sand porosity are referred to as "dirty sand" since they can contain up to 5% clay by volume (Figure 9). Calcarenite and siltstone are decompacted using the generalized curves of Bond and Kominz (1984). Only the lower limits of porosity were used for the backstripping analysis. Therefore, the relatively high porosities for sand and mud (Figure 7) will not affect the eustatic estimates discussed in the remainder of this study.

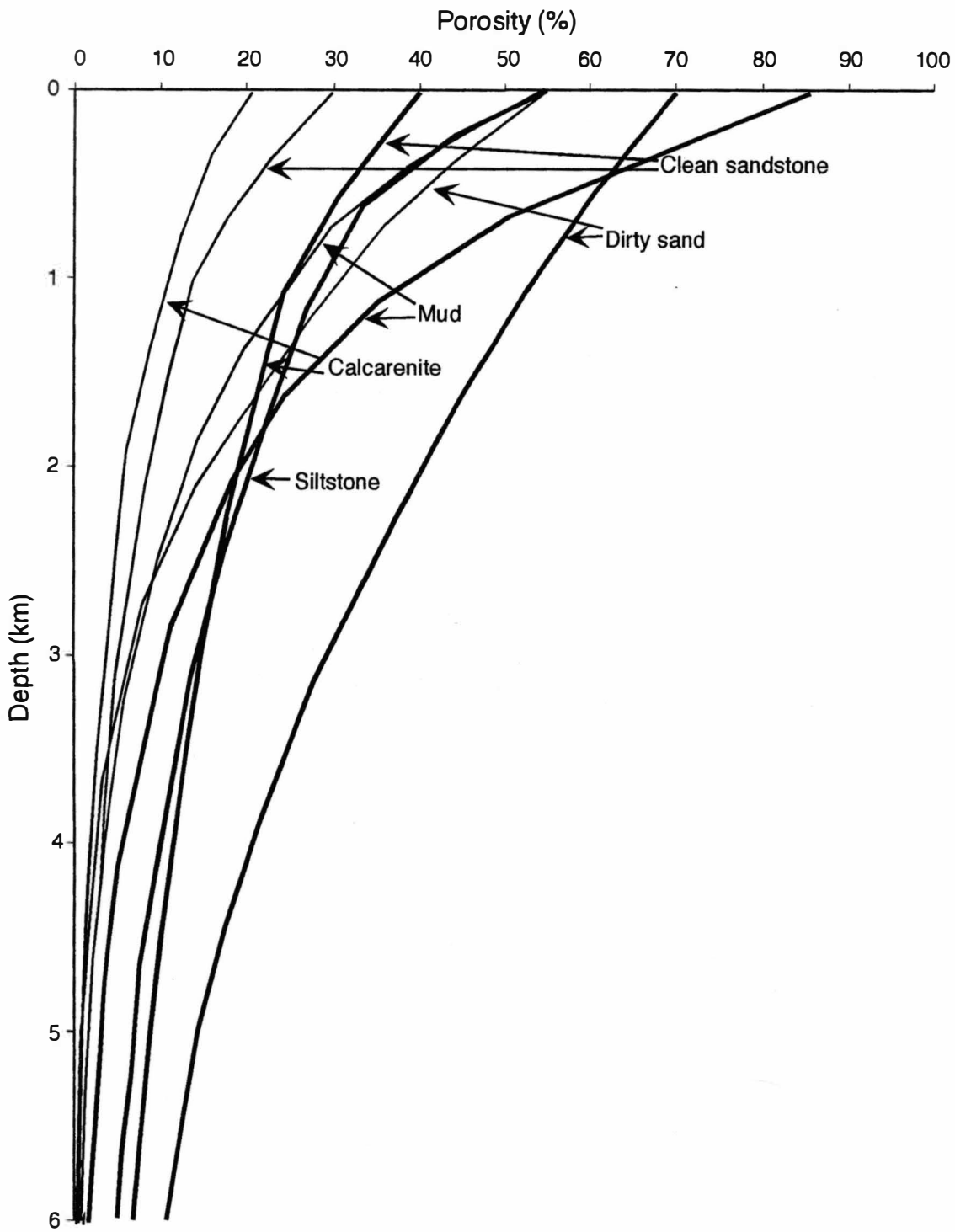

Figure 9. Empirical Porosity-Depth Curves Used for the Decompaction of the Bass River and Ancora Borehole Stratigraphy. Thin curves represent minimum values of decompaction and heavy curves represent maximum values of decompaction.

CHAPTER III

BACKSTRIPPING ANALYSIS

Introduction

Sequences are the fundamental building blocks of the stratigraphic record. The link between sequences and eustasy is controversial due to the complexity of the controls on sedimentation (tectonic subsidence, thermal cooling, sedimentation rates, sediment compaction, glacial ice volumes, etc.). Globally synchronous, sedimentary sequences bounded by unconformities constitute evidence for eustatic events (Vail, 1988). An eustatic signal is only recognized if it is large enough and is of worldwide extent (Kendall et al., 1992).

The backstripping method used in this study is a refinement of a procedure for analyses of subsidence in modern passive margins (Sleep, 1971; Steckler and Watts, 1978; Bond and Kominz, 1984). In this case, it is a one-dimensional analysis of post-rift sediments that contain evidence of eustatic events superimposed on the thermally controlled subsidence of the New Jersey margin (R1 curves). Most of the subsidence observed on the coastal plain is due to offshore sediment loading (Steckler et al., 1988). Because the New Jersey Coastal Plain is located on a mature passive margin, the form of subsidence is assumed to be that of a thermally subsiding basin. Theoretical thermal subsidence is assumed to be that of a cooling plate (McKenzie, 1978).

Once the effects of sediment loading, compaction, and thermal subsidence are removed, the remaining cause of subsidence, when compared globally, is assumed to be that of variations in sea level (R2 curves) if it is consistent in timing and amplitude.

Backstripping of stratigraphic data from previously drilled boreholes at Island Beach, Atlantic City, and Cape May (Figure 2) from the ODP-New Jersey Coastal Plain Drilling Project has revealed similar amplitudes in R2 curves (sea-level change) when sequences were represented in all three boreholes (Kominz et al., 1998). This suggests they isolated a possible eustatic signal since the magnitudes and duration of R2 were similar at different sites. Results of R2 revealed a long-term ($10^8 - 10^7$ years) eustatic fall of approximately 100 meters since early Eocene and suggested short-term (0.5 – 3 m.y.) eustatic rises and falls of less than 70 meters (Kominz et al., 1998). Although the magnitudes of both short and long-term sea-level estimates were considerably lower than those of Haq et al. (1987), the general trends were quite similar (Kominz et al., 1998).

Additional backstripping analysis of stratigraphic data from the Bass River and Ancora boreholes (Figure 2) was conducted to further determine if an eustatic signal had been isolated by the previous analysis (Kominz et al., 1998). In particular, more accurate porosity-depth relationships for sand and shale for these wells provided improved estimates of the magnitude of eustasy. Because these boreholes targeted older sequences of the Upper Cretaceous to Paleocene, new estimates of the magnitude of long-term sea-

level change was obtained along with new information on older (Cretaceous) short-term signals (Kominz et al., 1998).

Description of Boreholes

Bass River

The Bass River site is the fourth borehole drilled as part of the New Jersey Coastal Plain Drilling Project and the first site drilled as part of ODP Leg 174AX. It was continuously cored to a total depth of 596.34 m in October and November 1996 at Bass River State Forest, New Jersey (39°36'42" N, 74°26'12" W; elevation 8.53 m) (Miller et al., 1998). Drilling at Bass River targeted Middle Miocene and older strata, with the primary focus on Upper Cretaceous to Paleocene strata that previously were poorly sampled (Miller et al., 1998).

The thick stratigraphic section recovered at Bass River provides material relavent to various aspects of global change, regional tectonics, and local hydrogeology (Miller et al., 1998). The Bass River borehole is the first fossiliferous, continuously cored Upper Cretaceous section in New Jersey (Miller et al., 1998). It provides information needed for a detailed, integrated stratigraphic study of Cretaceous sequences (Miller et al., 1998).

Ancora

The Ancora borehole was the fifth site drilled as part of the New Jersey Coastal Plain Drilling Project and the second site drilled as part of ODP Leg 174AX. It was continuously cored to a total depth of 356.71 m in July and

August 1998 at Ancora, New Jersey (39°41'31.975" N, 74°50'56.459 W; elevation 31.65 m) (Miller et al., 1999). Two holes were drilled at Ancora: Hole A recovered 211.48 m of core between the surface and 231.34 m, while Hole B recovered 180.28 m of core between 165.5 m and a total depth of 356.71 m (Miller et al., 1999). The Ancora borehole was designed to sample up-dip equivalents of Upper Cretaceous strata sampled at Bass River and sample further into the Middle Cretaceous section (Miller et al., 1999).

The Ancora borehole was the most successful of the New Jersey Coastal Plain boreholes drilled in terms of recovery. The Upper Cretaceous section complimented the down-dip Bass River borehole in New Jersey, allowing reconstruction of sea-level variations for this interval and evaluation of sequence stratigraphic succession and facies models (Miller et al., 1999). The Ancora borehole persisted further into the Middle Cretaceous section providing new detailed stratigraphic data for this interval.

Lithostratigraphic Data

Backstripping requires detailed lithologic information from borehole stratigraphy (Appendix B, C). Lithologic descriptions (Miller et al., 1998; Miller et al., 1999) were supplemented by onsite physical characterization of core samples along with the relative percentages of quartz sand, silt-clay, glauconite, mica, and carbonate components through grain size analyses. Densities of units were calculated by the relative percent of lithologies (Equation 3).

$$D_G = [(.55 \times V_{clay\text{-}silt}) \times 2.7\ g/cm^3] + [(.35 \times V_{clay\text{-}silt}) \times 2.65\ g/cm^3] +$$
$$[(.10 \times V_{clay\text{-}silt}) \times 2.6\ g/cm^3] + [V_{sand} \times 2.65\ g/cm^3] +$$
$$[V_{glauconite} \times 2.6\ g/cm^3] + [V_{forams} \times 2.71\ g/cm^3] +$$
$$[V_{mica} \times 2.8\ g/cm^3]$$

Where

D_G = estimated grain density (g/cm^3)

V = volume (3)

The silt-clay fraction is assumed to be composed of 55% clay, 35% quartz, and 10% feldspar having densities of 2.7, 2.65, and 2.6, respectively. This assumption is made since the mineralogy of these sediments was not known.

Sequence bounding unconformities were identified by Miller et al. (1998) and Miller et al. (1999) on the basis of physical stratigraphy, including irregular contacts, reworking, bioturbation, major facies changes, gamma ray peaks, and paraconformities inferred from biostratigraphic and Sr isotopic breaks. Additional Sr isotopic analysis and paleowater depth estimates of borehole stratigraphy at Bass River and Ancora were acquired after publication of the site reports (Miller et al., 1998; Miller et al., 1999). This data was provided by Ken Miller, Richard Olsson, Steve Pekar, and Ben Cramer at Rutgers University along with Jim Browning at the University of North Carolina. This data assisted in dating sequences and further establishing additional sequence boundaries. Paleowater-depth estimates were derived from benthic foraminiferal assemblages and sedimentary facies analyses.

Analyses of sedimentary facies were used for shallow water environments with no fossil preservation.

Cretaceous age sequences are tied to the Gradstein et al. (1995) time scale and Cenozoic age sequences are tied to the Berggren et al. (1995) time scale using integrated magnetostratigraphy, Sr isotopic stratigraphy, and biostratigraphy. Ages were assigned to the top and base of each sequence using the recent Sr data. The ages of intermediate points were obtained via linear interpolation of decompacted sediment thickness (e.g., Kominz et al., 1998). Because a more detailed estimate of ages within sequences is beyond the accuracy of our age control, sedimentation rates are assumed to be constant although they were no doubt variable (Miller, 1997). Lowstand systems tracts (LST) on the coastal plain are generally absent and sequences represented stacked transgressive (TST) and highstand (HST) systems tracts (Miller et al., 1996).

Lithostratigraphy and sequence stratigraphy for the Bass River and Ancora boreholes were generated from detailed borehole stratigraphy (Figures 10,11). The correlation of borehole stratigraphy illustrates the sequence stratigraphic framework of boreholes perpendicular to the original margin with sedimentary packages generally thickening and prograding seaward (Figures 12,13). The Bass River and Ancora boreholes clearly show sampling of older sequences (Paleocene to Upper Cretaceous) in a more up-dip direction compared to the previously drilled boreholes (ODP Leg 150X).

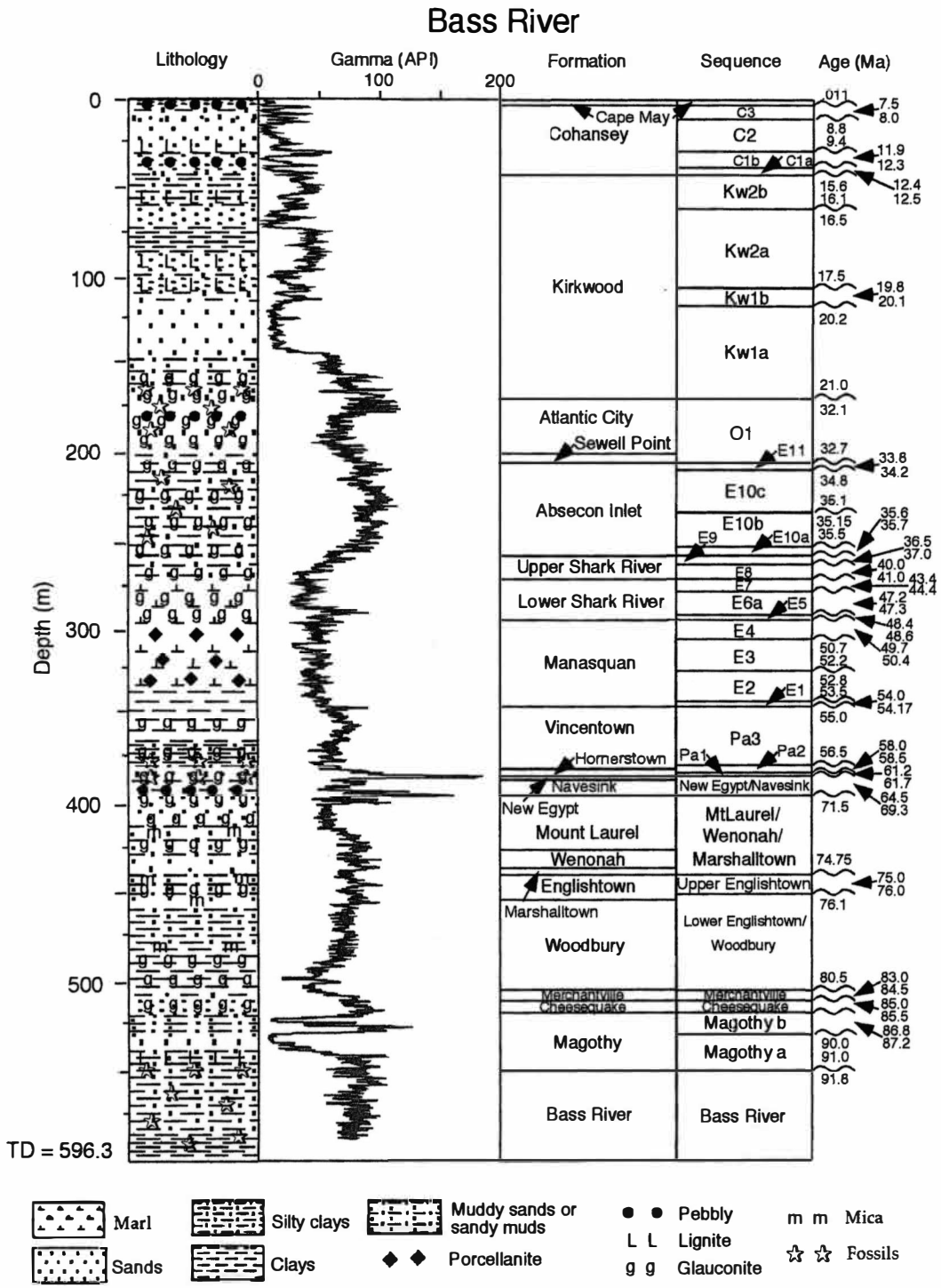

Figure 10. Lithostratigraphic and Sequence Stratigraphic Description of the Bass River Borehole.

Source: Data from Miller et al. (1998). Ages of sequences from Appendix B.

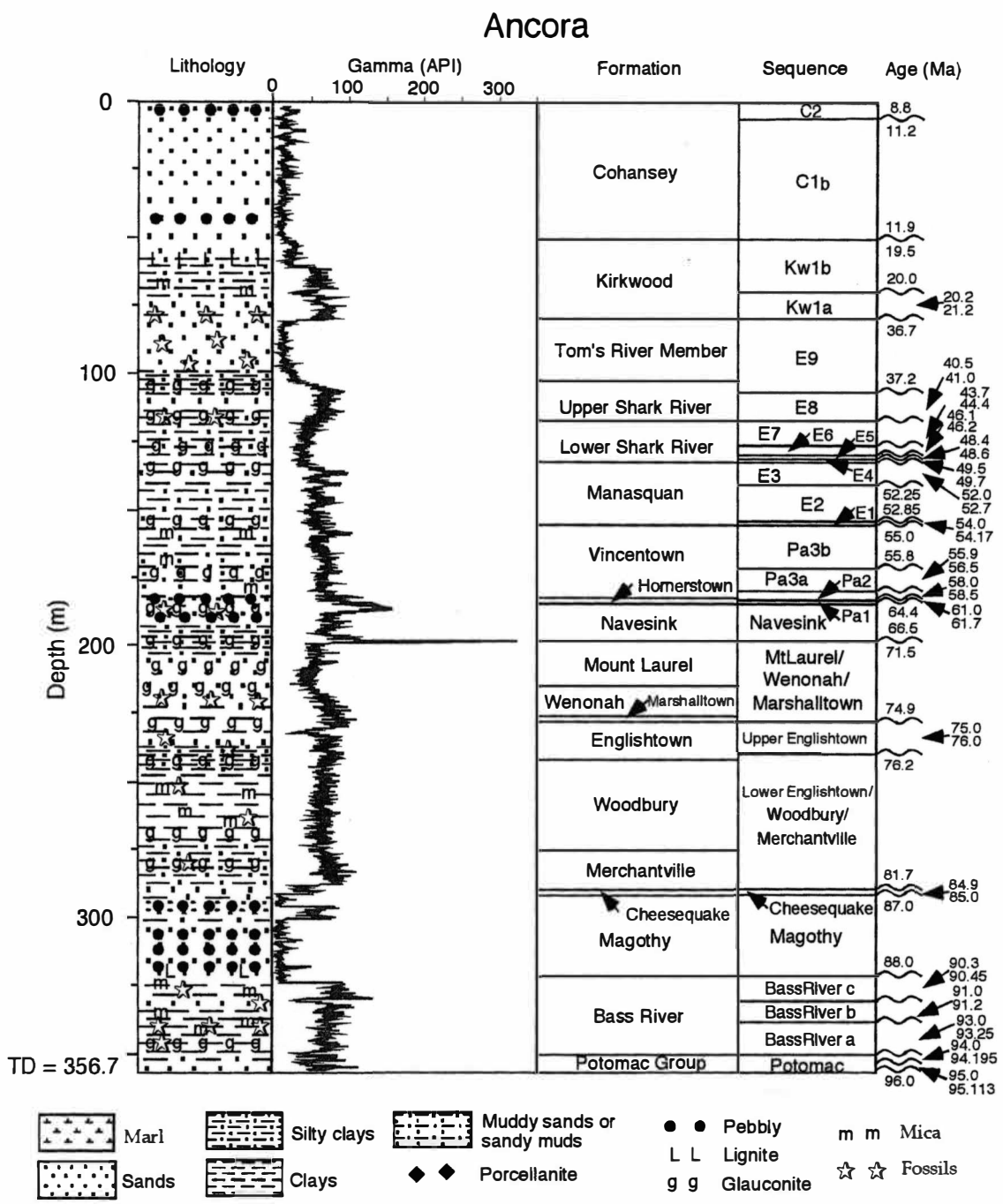

Figure 11. Lithostratigraphic and Sequence Stratigraphic Description of the Ancora Borehole.

Source: Data from Miller et al. (1999). Ages of sequences from Appendix C.

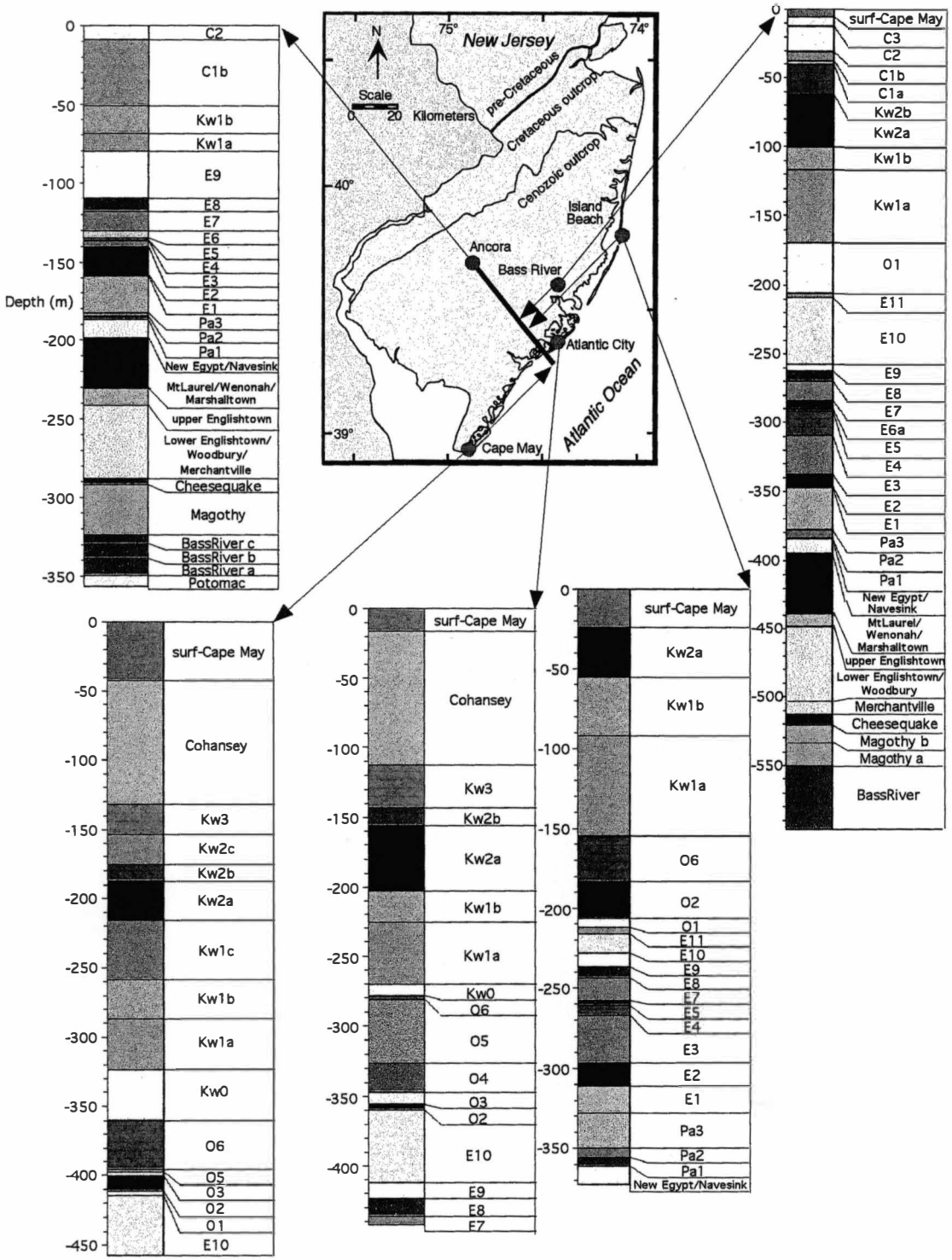

Figure 12. Strip Logs of Sequences for the Five Boreholes (ODP Legs 150X & 174AX) and Map Showing Location of Boreholes Along Projected Dip-Section for Figure 13.

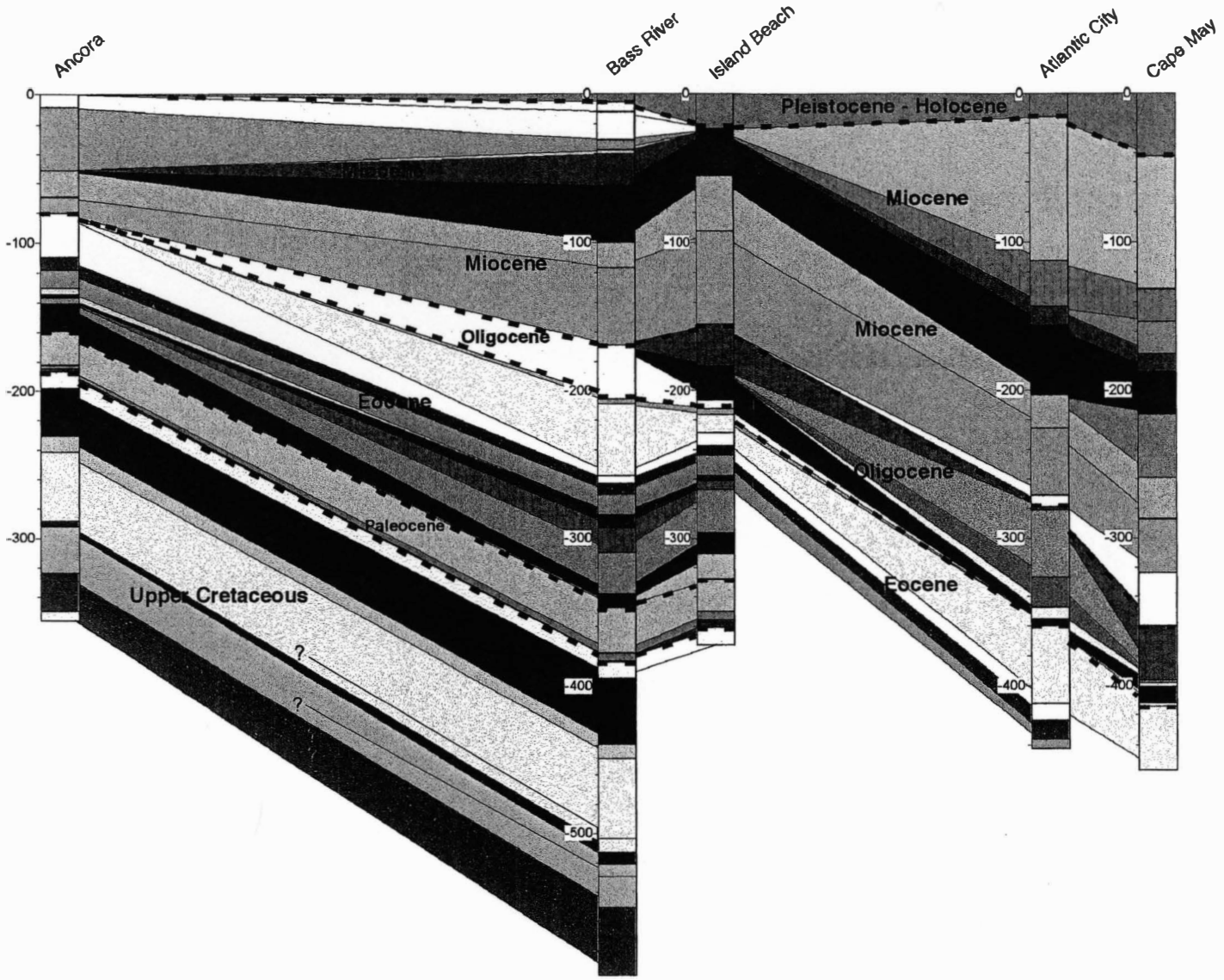

Figure 13. Projected Dip Cross-Section Illustrating the Sequence Stratigraphic Framework of Boreholes on the New Jersey Coastal Plain. Individual colors represent sequences. Dashed lines represent time lines between epochs.

Strata Beneath the Bass River and Ancora Boreholes

Backstripping requires stratigraphic information to the basement to account for accommodation due to compaction and to evaluate the amplitude of long-term eustatic change (Kominz et al., 1998). Thickness of strata beneath the Bass River and Ancora boreholes were estimated via linear interpolation between well/borehole sites. At Bass River, 20 meters of Bass River Formation was added by interpolating its thickness between the Ancora borehole and the Island Beach well #33-10131 while 409 meters of Potomac Formation was added by interpolating between the Clayton-1 well and Island Beach well #33-01031. At Ancora, 332 meters of Potomac Formation was added by also interpolating between the Clayton-1 well and Island Beach well #33-01031.

The basal sequence of sediments in the coastal plain outcrop is the Potomac Group of Early Cretaceous age (Olsson et al., 1988) overlain by the Bass River Formation. At the Bass River, 45.75 m of Bass River Formation was drilled to the base of the borehole (Miller et al., 1998). At Ancora, the entire Bass River Formation was encountered (26.2 m) and 6.7 m of Potomac Group was drilled to the base of the borehole (Miller et al., 1999).

The thickness of Bass River Formation beneath the Bass River borehole was calculated via linear interpolation between the Ancora borehole and Island Beach well #33-01031 (Figure 14, 15). The Bass River Formation at the Island Beach well #33-01031 is 93 m thick (Gill et al., 1963). Lithologic descriptions for the basal-most Bass River Formation were taken from the Ancora borehole (Miller et al., 1999).

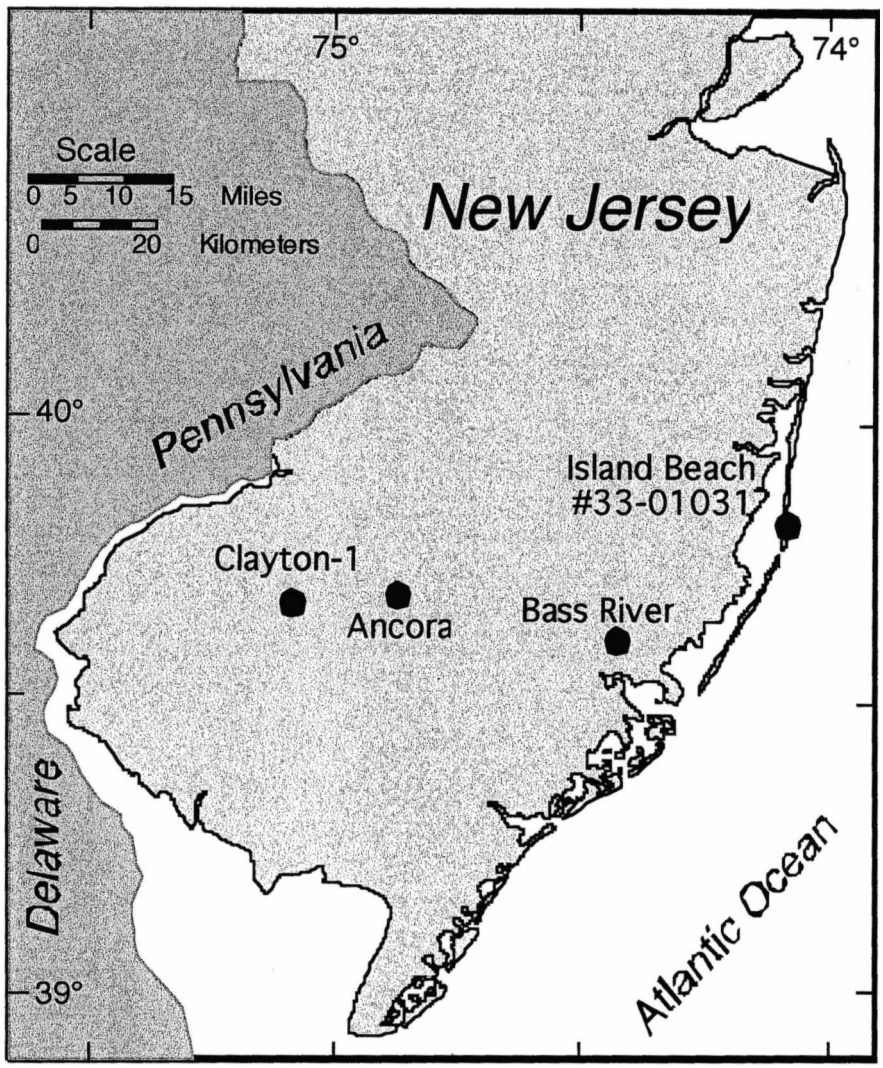

Figure 14. Location of Boreholes/Wells Used to Estimate Thickness of Strata to Basement Beneath the Bass River and Ancora Boreholes.

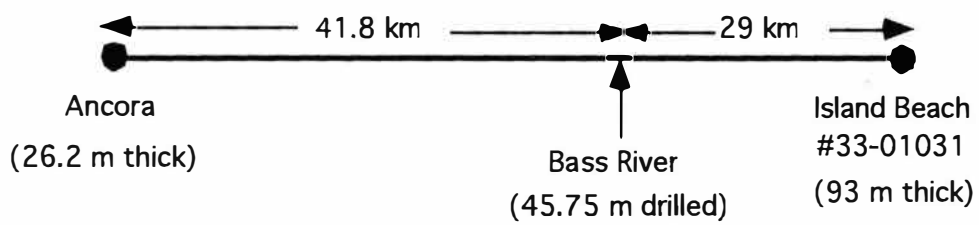

Figure 15. Schematic Representation Used to Estimate Thickness of Bass River Formation Beneath the Bass River Borehole.

$$z = \left[93\ \text{m} - \left[29\ \text{km}\left[\frac{93\ \text{m} - 26.2\ \text{m}}{41.8\ \text{km} + 29\ \text{km}}\right]\right]\right] - 45.75\ \text{m} \approx 20\ \text{m} \quad (4)$$

The thickness of Potomac Group beneath the Bass River and Ancora boreholes were calculated via linear interpolation between the Clayton-1 well and Island Beach well #33-10131 (Figure 14, 16). The Potomac Group at the Clayton-1 well is 298.7 m thick (Owens et al., 1998) and 460 m thick at the Island Beach well #33-01031 (Olsson et al., 1988). The Potomac Group is interpreted as a complex of fluvial-deltaic lithofacies which include braided and meandering stream sands and gravels, upper flood plain, lower floodplain, and fringing swamp deposits (Olsson et al., 1988).

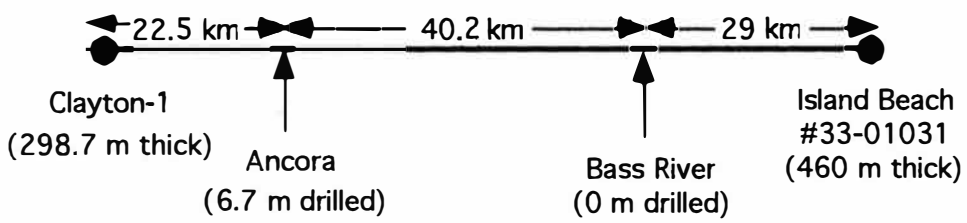

Figure 16. Schematic representation used to estimate thickness of Potomac Group beneath the Bass River and Ancora boreholes.

$$z = \left[460\ \text{m} - \left[29\ \text{km}\left[\frac{460\ \text{m} - 298.7\ \text{m}}{22.5\ \text{km} + 40.2\ \text{km} + 29\ \text{km}}\right]\right]\right] - 0\ \text{m} \approx 409\ \text{m} \quad (5)$$

$$z = \left[298.7\ \text{m} + \left[22.5\ \text{km}\left[\frac{460\ \text{m} - 298.7\ \text{m}}{22.5\ \text{km} + 40.2\ \text{km} + 29\ \text{km}}\right]\right]\right] - 6.7\ \text{m} \approx 332\ \text{m} \quad (6)$$

The Backstripping Method

Backstripping is a quantitative method of estimating tectonic subsidence of a basin, which is the basement's vertical movement in the absence of sediment and sea-level change. We employ the traditional, one-dimensional analysis that assumes an Airy isostatic model where the basement response to load is directly beneath the load (Bond et al., 1989). The calculation of tectonic subsidence is given by the general equation developed for modern sedimentary basins (Steckler and Watts, 1978).

$$TS = \left[S^* \left(\frac{\rho_a - \rho_s}{\rho_a - \rho_w} \right) - \Delta SL \left(\frac{\rho_w}{\rho_a - \rho_w} \right) \right] + WD - \Delta SL$$

Where

TS = tectonic subsidence

S* = decompacted sediment thickness

ρ_a = mean density of asthenosphere (3.40 g/ cm^3)

ρ_s = mean grain density of sediments

ρ_w = mean density of sea water

ΔSL = change in eustatic sea level

WD = paleowater depth (7)

Decompacted sediment thickness is calculated using low and high end-member porosity-depth curves for mud, sand, calcarenite, and siltstone. Relative percentages of these lithologies were calculated from cumulative percentages of grain components (Appendix B, C).

Mud is assumed to include 80% of the volume of clay-silt component.

$$\% \text{ Mud} = .80 \times V_{\text{clay-silt}} \quad (8)$$

Sand includes the total volume of the sand, glauconite, and mica components. Both glauconite and mica are assumed to compact like sand. Because the percentage of mica is relatively low, this assumption is fair to say.

$$\% \text{ Sand} = V_{\text{sand}} + V_{\text{glauc.}} + V_{\text{mica}} \quad (9)$$

Siltstone is assumed to include 20% of the volume of the clay-silt component.

$$\% \text{ Siltstone} = .20 \times V_{\text{clay-silt}} \quad (10)$$

Calcarenite includes the total volume of the calcareous components.

$$\% \text{ Calcarenite} = V_{\text{forams}} \quad (11)$$

Porosities from the Cost B-2 well (Rhodehamel, 1977) along with new porosity data (Chapter 2; Figure 6) were used for sand and mud. Carbonates and siltstones were decompacted using the generalized curves of Bond and Kominz (1984).

If the tectonic component of subsidence is known, a modification of the backstripping method can be used to estimate the magnitudes of the eustatic component. This modification involves quantitative reductions of stratigraphic data. The first reduction (R1) removes the effects of sediment loading and compaction producing curves that are an approximation of the subsidence that would have occurred if the basin had subsided in water and without deposition of sediment (Bond and Kominz, 1991).

$$R1 = TS + \Delta SL\left(\frac{\rho_a}{\rho_a - \rho_w}\right) = S*\left(\frac{\rho_a - \rho_s}{\rho_a - \rho_w}\right) + WD \tag{12}$$

Because the tectonic component of subsidence along the New Jersey margin is that of a cooling plate, the best-fit McKenzie (1978) curves for a cooling lithospheric plate are subtracted from R1 curves producing a second set of curves, designated R2 (second reduction). Once the effects of sediment loading, compaction, and thermal cooling are removed, the remaining factor of subsidence includes variations in sea level as well as any non-thermal component of R1. If the magnitudes and duration of R2 are similar when sequences are represented from different borehole sites, the result may be taken to represent eustasy.

$$R2 = (R1 - TS)\left(\frac{\rho_a - \rho_w}{\rho_a}\right) \tag{13}$$

The form of subsidence along the margin was that of a thermally subsiding basin because most or all of the subsidence observed on the coastal plain was due to the flexural response to offshore sediment loading (Steckler et al., 1988). This flexural response created sufficient accommodation onshore for sediment accumulation to occur on the coastal plain. Theoretical thermal subsidence was assumed to be that of a cooling plate (McKenzie, 1978). Thermal subsidence was calibrated to an ocean floor with a thermal decay constant of 36 million years and an equilibrium plate thickness of 95 kilometers (Stein and Stein, 1992). Best-fit thermal subsidence was calculated

by first fitting an exponential curve with a decay constant of 36 million years by linear regression (Kominz et al., 1998). The best-fit value of the exponential fit at 0 million years was used to constrain a best-fit stretching factor (Kominz et al., 1998). Initial thermal subsidence was assumed to start at 150 million years ago after the formation of the passive margin (Steckler et al., 1988; Olsson et al., 1988).

Backstripping Results

The variation in subsidence (R1) that resulted when the low end-member porosity-depth curves were applied were compared from the R1 results obtained by applying the high end-member porosity-depth curves in the Bass River borehole (Figure 17). The R1 curve using high end-member porosity-depth curves shows the most subsidence. This is a result of the increase in volume of water (water loading) due to the increase volume of pore spaces. On average, the R1 curve using high end-member porosity-depth curves shows approximately 160 m more subsidence compared to the R1 curve using low end-member porosity-depth curves. Although the variation in R1 is 160 m, the variation in R2 curves is quite low (Figure 18). Thus, the magnitude of long-term eustatic sea level is moderately dependent on porosity while the magnitude of 3rd order eustatic sea level is most dependent on paleowater depth. In order to be consistent with previous results of Kominz et al. (1998), R1 and R2 results using low end-member porosity-depth curves will be used for discussion in the remainder of this study.

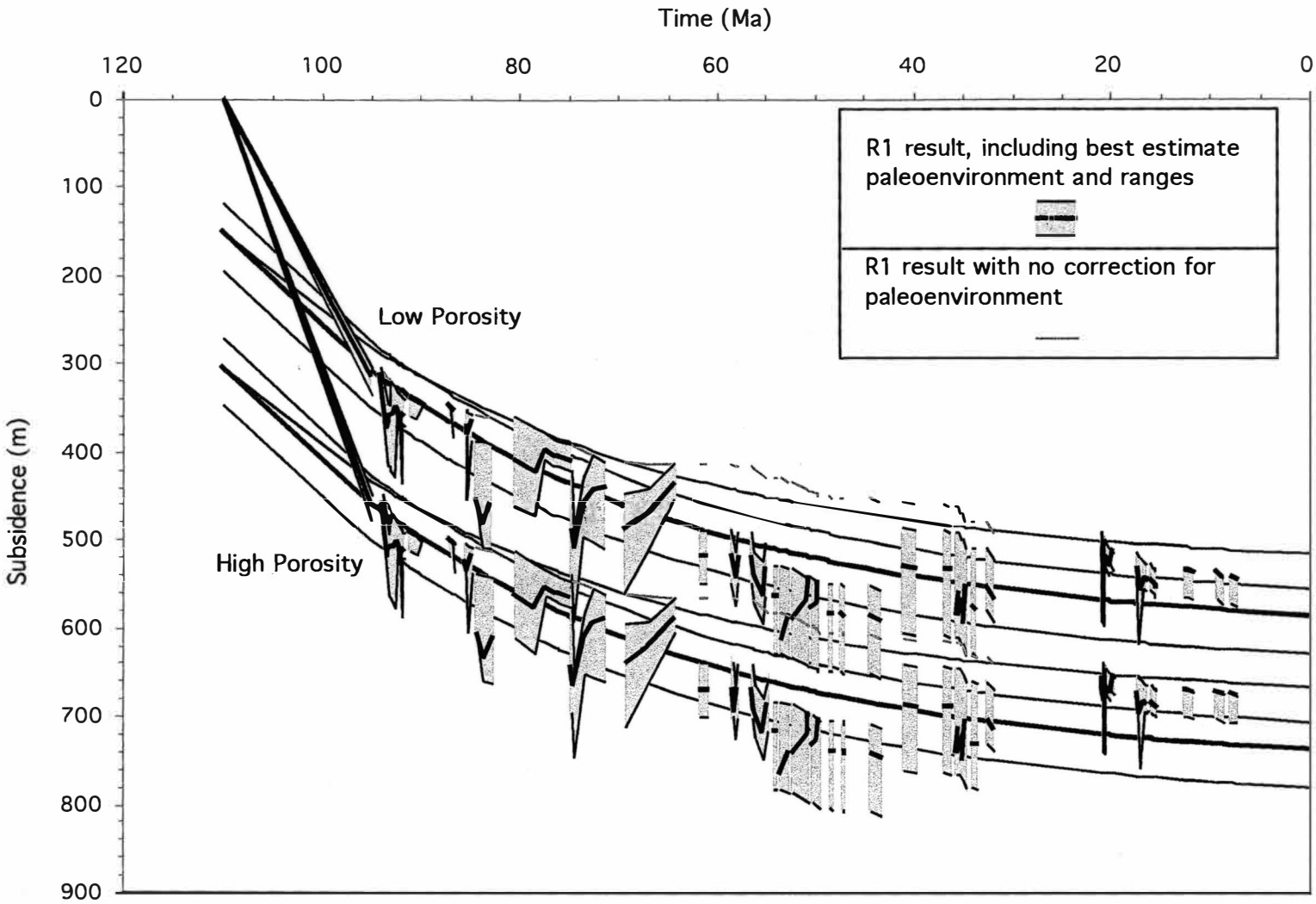

Figure 17. R1 Results for the Bass River Borehole Using High and Low End-Member Porosity-Depth Curves.

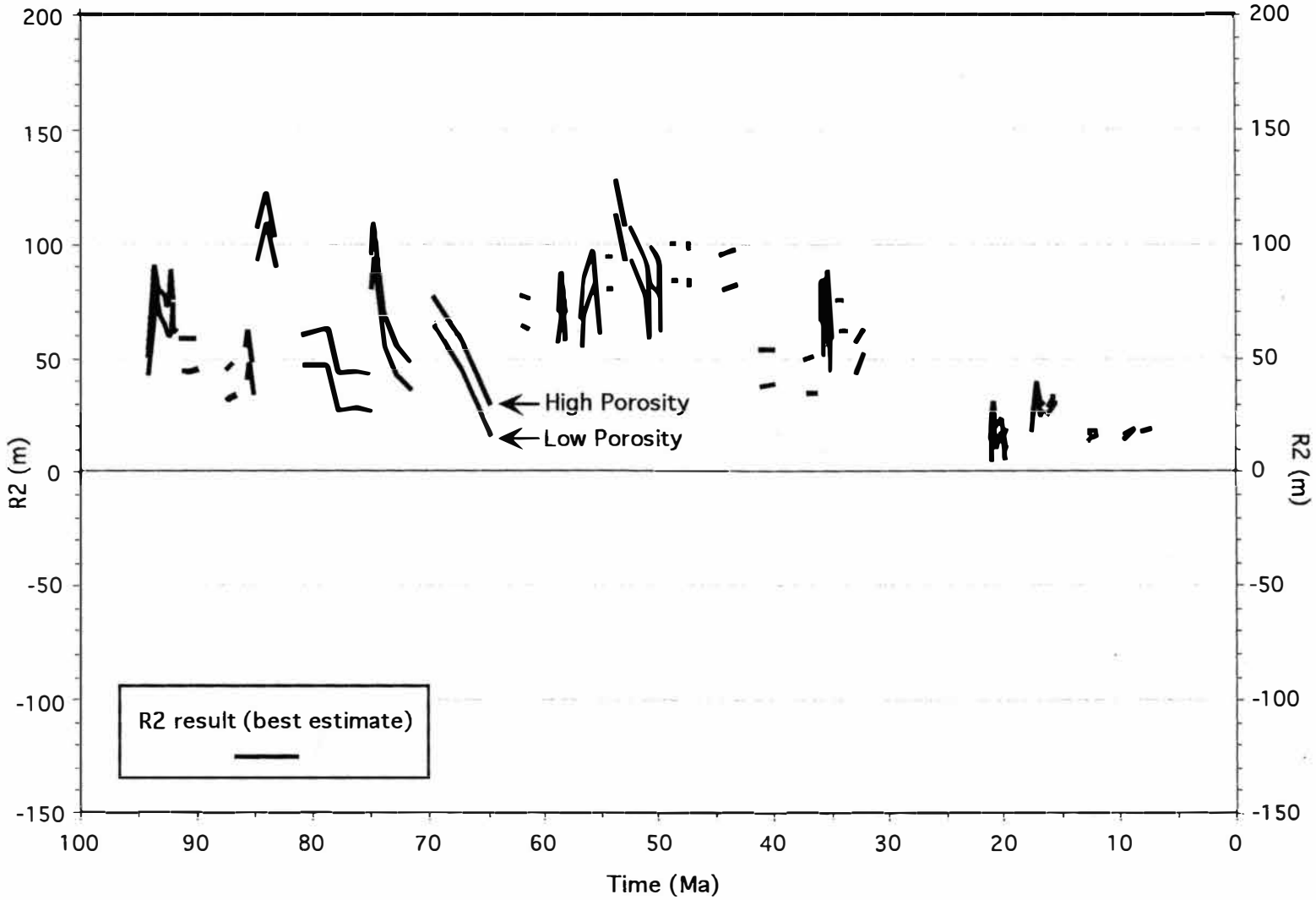

Figure 18. R2 Results for the Bass River Borehole Using High and Low End-Member Porosity-Depth Curves.

The R1 curves (Figure 19) show the subsidence that occurred in the Bass River and Ancora boreholes using low end-member porosity-depth curves. The solid curves (red and blue) represent thermal curves fit to the R1 curves. The R1 curves are plotted where sediment is present and gaps represent hiatuses (sequence boundaries). R1 curves younger than 95 m.y. represent cored borehole data. Older R1 curves represent estimated stratigraphy beneath the boreholes to basement depth. In general, subsidence at Bass River was greater than that at the Ancora site. More subsidence occurs at Bass River because it is located in a more down-dip direction from Ancora, thus containing a thicker sequence of sediments. Bass River also has the greatest stretching factor (β) or ratio of stretched to pre-stretched lithosphere thickness. This is only an indication of relative magnitudes of subsidence since stretching factors are one (no stretching) beneath the coastal plain.

Overall, the trends of R2 (Figure 20) for both the Bass River and Ancora boreholes are consistent between sequences, although the magnitudes do vary. The magnitudes of R2 between sequences (assuming best-estimate paleodepths) vary by as much as 50 m between the two boreholes. This predominately occurs in the new Cretaceous and Paleocene data. The variation of R2 between sequences seem to decrease from the Eocene through Holocene where the magnitudes differ by a maximum of 30 m, but usually differ by only 15 m.

The variation of R2 across sequence boundaries dominately occurs in

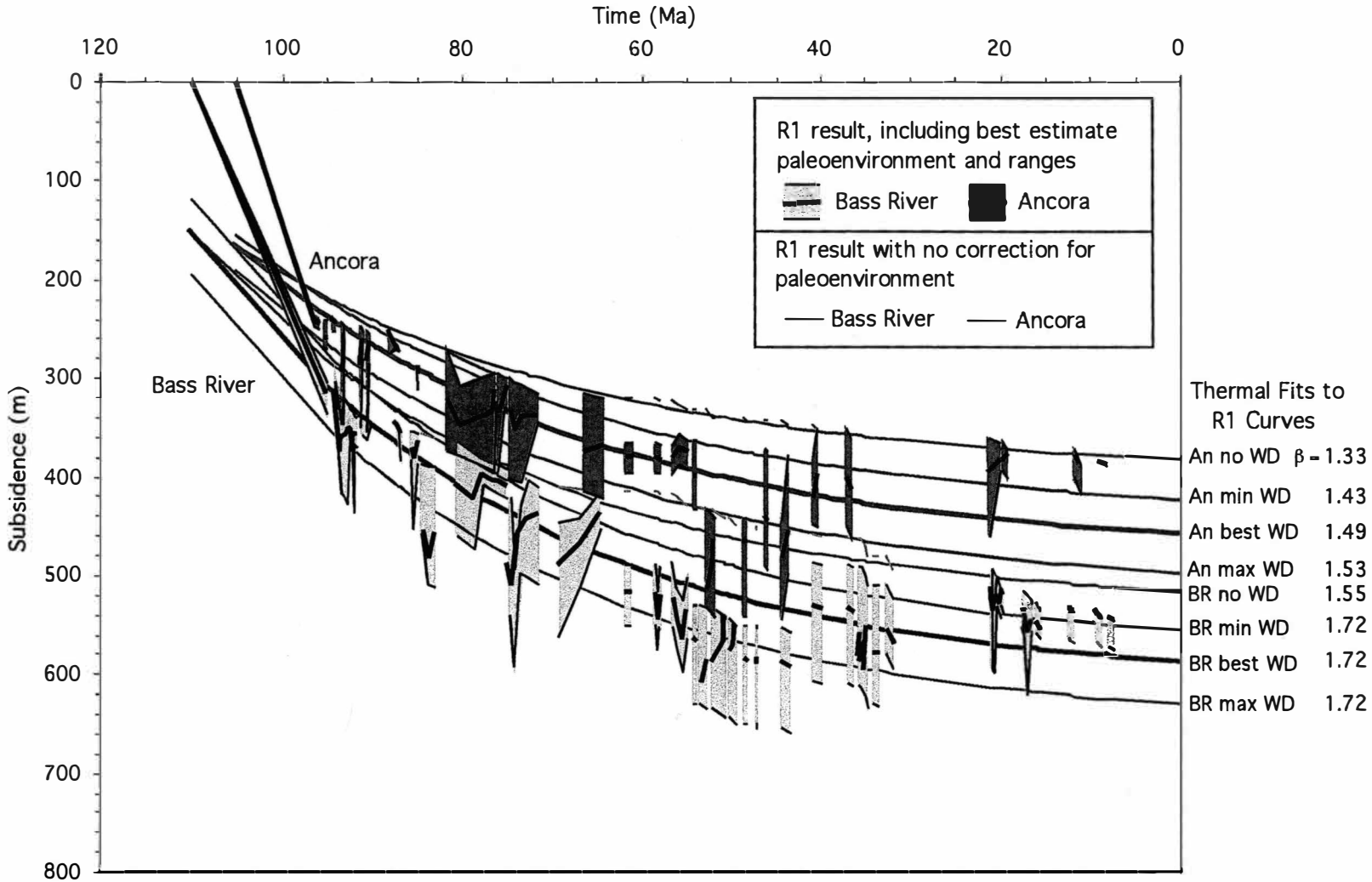

Figure 19. R1 Results for the Bass River and Ancora Boreholes (WD = water depth and β = stretching factor).

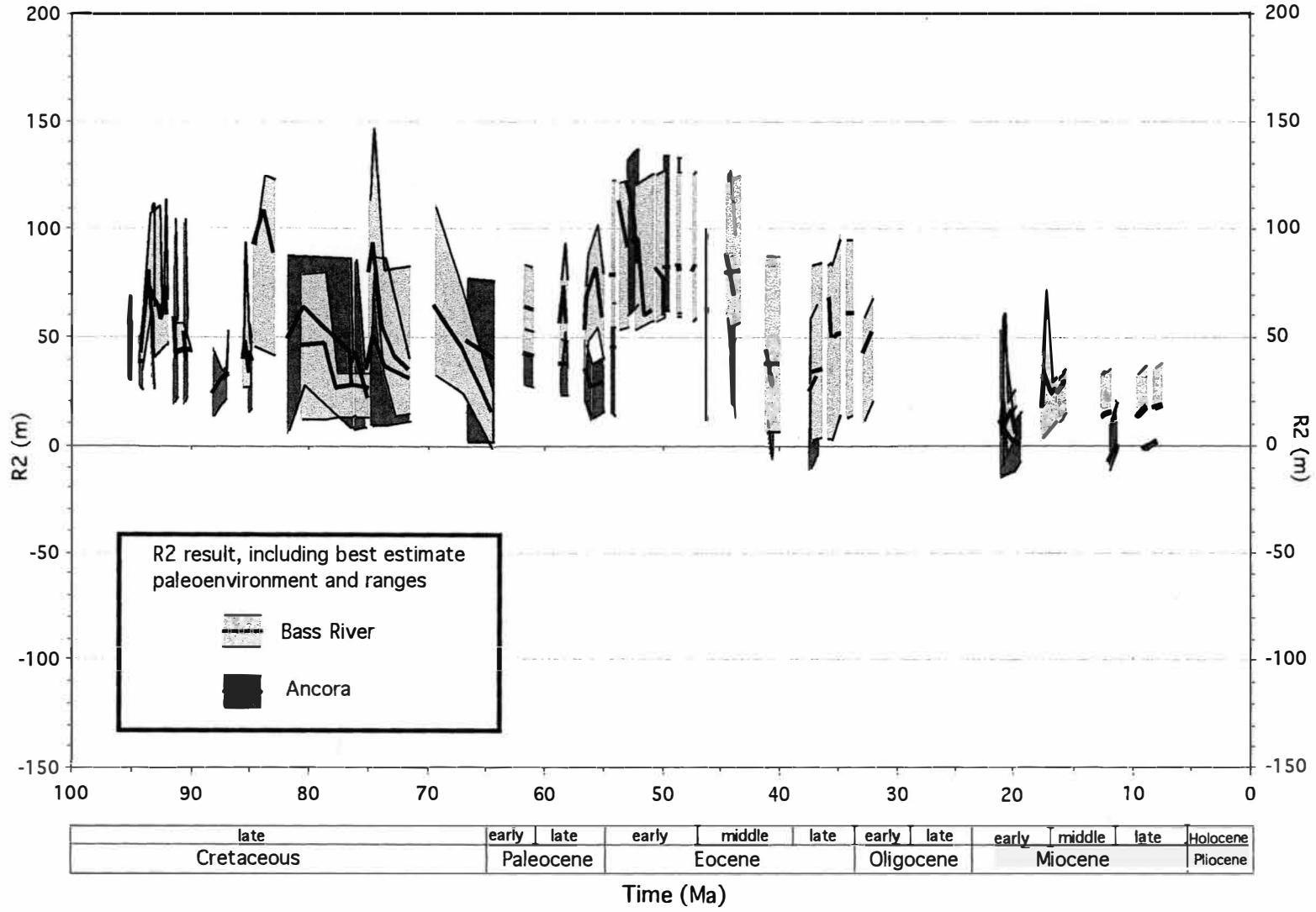

Figure 20. R2 Results for the Bass River and Ancora Boreholes.

the new Cretaceous data that vary by as much as 50 m. Although some variation occurs across sequence boundaries in the Paleocene, an overall increase in R2 takes place from early to late Paleocene and into the early Eocene (assuming ranges of paleodepths). A maximum in R2 occurs in the early Eocene with a maximum magnitude of about 130 m (assuming best-estimate paleodepth). Assuming the ranges of paleodepths, an overall decrease in R2 takes place through the Eocene. A possible peak in R2 may occur in the late Eocene. A long hiatus (≈ 11 m.y.) takes place throughout most of the Oligocene followed by deposition in the early Miocene. Variation in the magnitudes of R2 occurs in the middle to late Miocene where Bass River is greater in magnitude by about 20 m. A more detailed description of results are discussed in the following chapter.

CHAPTER IV

DISCUSSION

The R2 curves for Bass River and Ancora (Figure 21) are plotted with R2 data of Kominz et al. (1998) to establish if an eustatic signal has been isolated. The overall trends of R2 for Bass River and Ancora are consistent with Island Beach, Atlantic City, and Cape May. Where they overlap, the magnitudes and duration of R2 for the new boreholes are quite similar to previous boreholes. This suggests that an eustatic signal has been isolated. In most instances, the best estimates for Bass River and Ancora fall within the ranges of R2 for the other boreholes.

The R2 curves reveal considerable variability in the amplitudes of 3rd order (0.5 – 3 m.y.) sea-level changes. This is true for the new Cretaceous eustatic curves (Figure 22) which may be offset by as much as 50 m (assuming best-estimate paleodepths) between boreholes. Assuming that about half of the eustatic signal is captured in the TST and HST, the maximum amplitude of 3rd order sea-level change was about 90 m. The R2 curves of the Cretaceous illustrate the expected pattern for TST and HST (e.g., Cheesequake and Merchantville sequences; Figure 22). Assuming best-estimate paleodepths, the curves should increase during a transgressive event followed by a decrease in R2 during a regressive event. It is appropriate to imagine the R2 curves dipping downward in the gaps between the observed sequences since

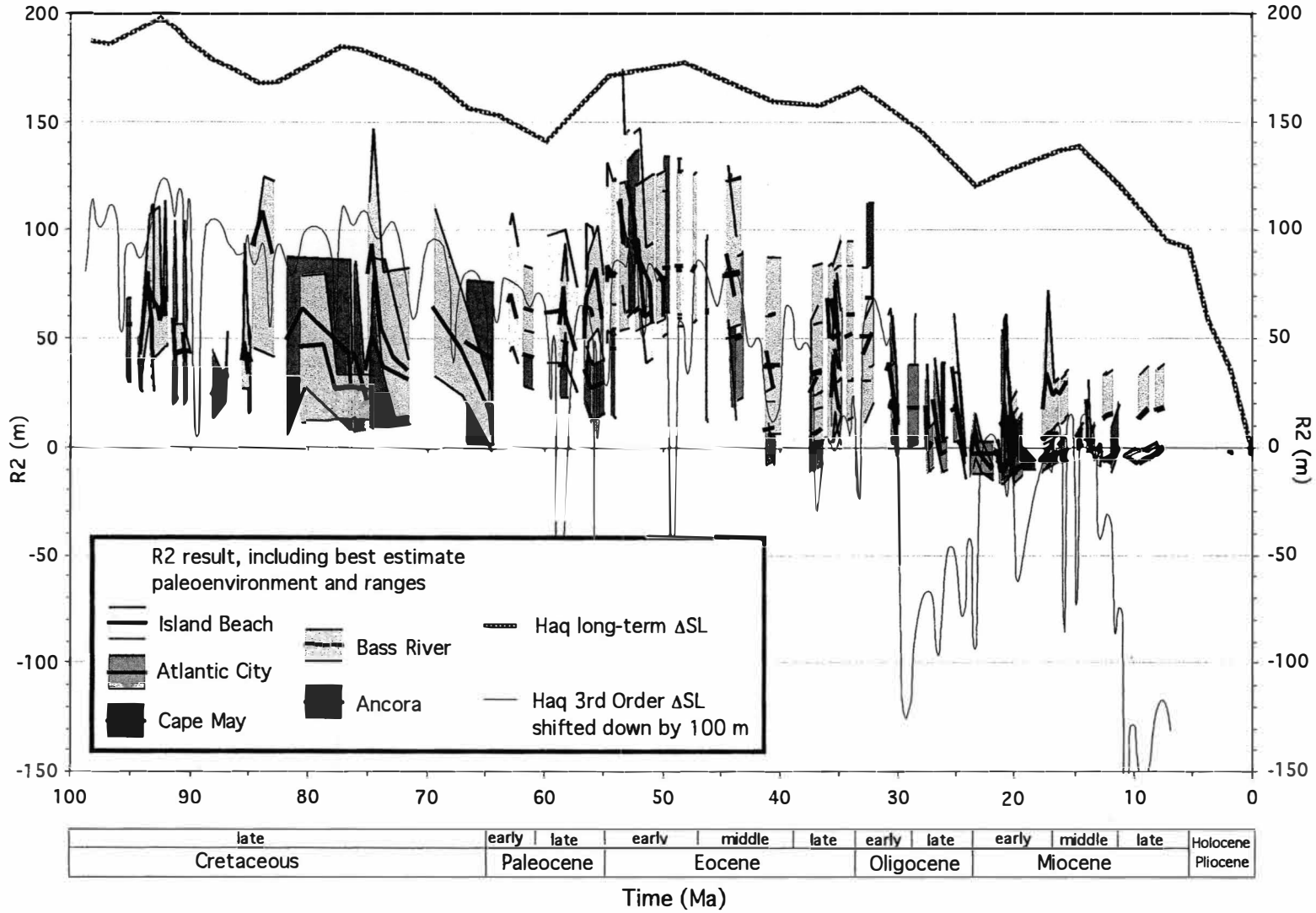

Figure 21. R2 Results for the Five Boreholes. Also plotted are long-term and 3rd order sea-level curves of Haq et al. (1987). The 3rd order sea-level curve of Haq et al. (1987) is shifted down 100 m.

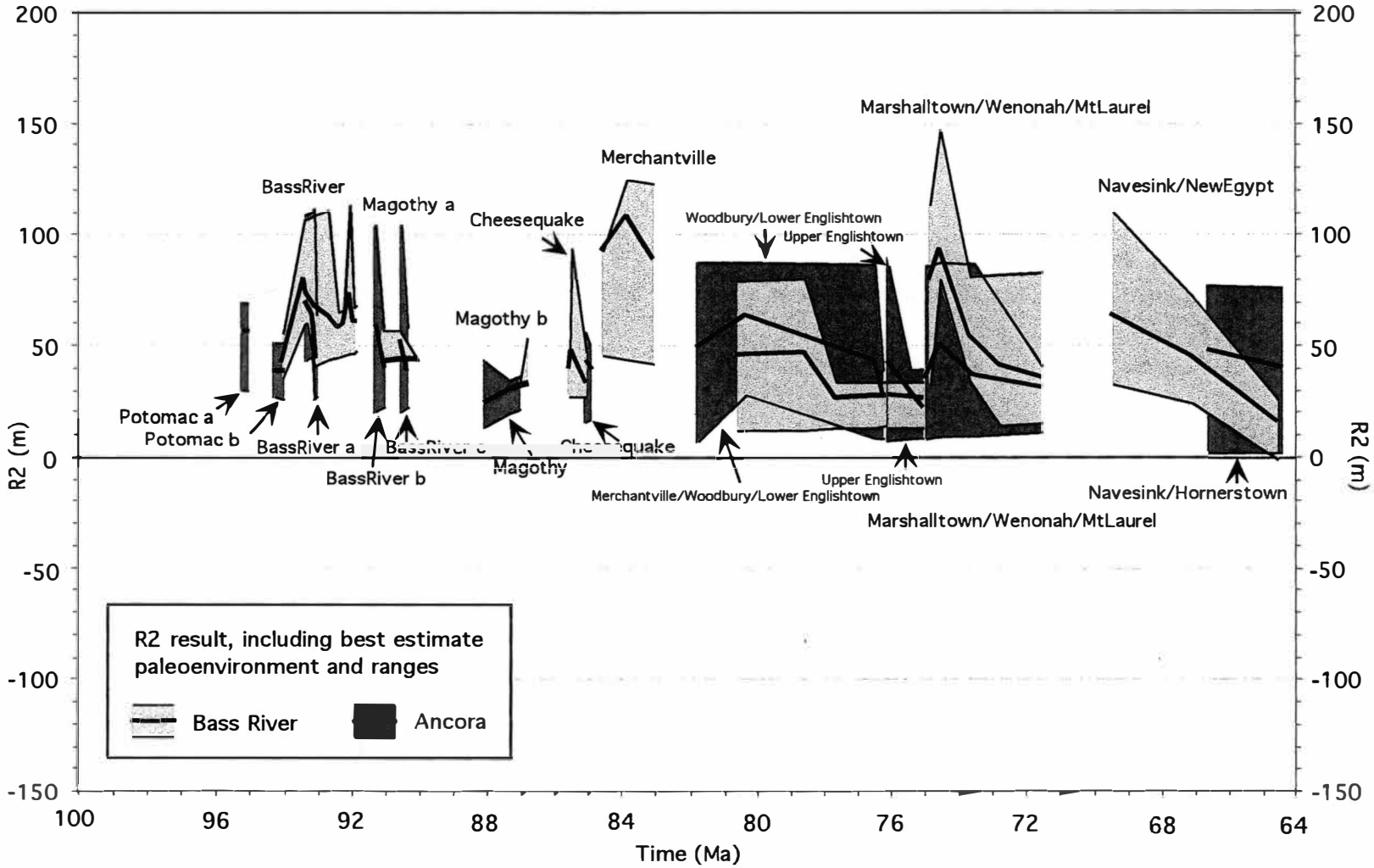

Figure 22. R2 Results for Upper Cretaceous Age Sequences. Names of sequences in the new Cretaceous data are given by names of the formations present in the sequence. Therefore, names of the same sequence may differ between borehole sites.

lowstand deposits were absent (e.g., Kominz et al., 1998).

The Potomac a sequence represents the oldest sequence from these two boreholes. Sequences from the Ancora borehole shows an increase in unconformities and a decrease in preservation. This is expected to occur in boreholes located in more onshore positions. Evidence of such patterns can be seen in the Potomac b and Bass River sequences at Bass River. A hiatus occurs at Ancora while deposition continues at Bass River. A similar trend occurs between the Magothy a, Bass River b and Bass River c sequences. The R2 curve for the Magothy a sequence does not show the regressive events evident in the Bass River b and c sequences. This is problematic when considering the expected results for this sequence stratigraphic model.

The Magothy b and Magothy sequences are consistent in magnitude, but are inconsistent in duration. Deposition of the Magothy b sequence does not occur until deposition of the Magothy sequence ceases. Deposition of the Magothy b sequence should continue during the duration of the Magothy sequence. The Cheesequake sequence is also inconsistent where deposition at Ancora occurs where deposition at Bass River ceases.

A hiatus of about 3 million years occurs at Ancora during deposition of the Merchantville sequence at Bass River. The variation in the magnitude of R2 across the sequence boundaries remain quite low (≈20 m) from 95 to 87 m.y. The magnitude of R2 increases from about 40 m in the Cheesequake sequence to about 90 m in the Merchantville sequence. A decrease in the magnitude of R2 then occurs from about 90 m in the Merchantville sequence to about 50 m across the sequence boundary. The R2 curve for the

Woodbury/ Lower Englishtown sequence at Bass River is consistent to that at Ancora although the magnitudes slightly vary. Deposition at Ancora also occurs before deposition at Bass River. The magnitude of R2 across the sequence boundary to the Englishtown sequence is similar. The R2 of the Upper Englishtown sequence is consistent in duration, but does not show the consistent trends.

The variation in magnitude of R2 across the sequence boundary (Upper Englishtown to Marshalltown/ Wenonah/ MtLaurel) is quite low at Ancora, but is as much as 50 m at Bass River. The R2 curves of the Marshalltown/ Wenonah/ MtLaurel sequence are consistent in trend, but vary in magnitude by as much as 40 m. The variation in magnitude of R2 across the sequence boundary (Marshalltown/ Wenonah/ MtLaurel to Navesink/ New Egypt) is about 30 m. The Navesink/ New Egypt sequence at Bass River reveal the similar trend to the Navesink/ Hornerstown sequence at Ancora, but the timing is inconsistent to the expected stratigraphic model. Again, deposition at Bass River cannot occur unless there is deposition at Ancora.

Although the amplitudes within sequences vary, the trends of R2 between boreholes in the Upper Cretaceous are remarkably similar. The inconsistencies in the timing and duration of R2 for sequences from the new Cretaceous data may be partly due to the age uncertainty (0.7 m.y.) in the Sr isotopic analysis. Other non-thermal factors affecting the magnitude and duration of R2 may be due to varied rates of sedimentation which can affect

the pre-existing geometry of the paleoshelf edge (e.g. delta lobe switching). Varied sedimentation rates may be caused by local tectonics and local climate.

It must be noted that the names of sequences from the new Cretaceous data are given by names of the formations present in the sequence. This was done before the backstripping analysis, thus, without a clear picture as to the spatial distribution of sequences with time. Therefore, names of the same sequence may differ between borehole sites, even though they represent the same sequence. Once the backstripping analysis had been done, the distribution of sequences, with respect to time, is more apparent (Figure 22). An example is the Magothy a sequence in Bass River that is present at the same time as the BassRiver b and BassRiver c sequences. Even though they have different names, Sr data shows that they represent sequences that were deposited at the same time.

The eustatic amplitudes between boreholes in the Paleocene (Figure23) are also variable between sequences, although the trends are quite similar. The variation of the magnitude or R2 across the sequence boundaries are quite low (≈20 m) in the Paleocene. The offset of the age sequence Pa1 at Island Beach could be due to age uncertainties (± 0.7 m.y.) in Sr isotopic analysis. It could also represent a separate sequence, but another sequence at Island Beach should be present at the same time as Pa1 at Bas River and Ancora. Sequence Pa2 is consistent in timing although the magnitude at Ancora is lower. Sequence Pa3 at Ancora actually represents two sequences. Again, this is expected in boreholes located in more onshore positions. The magnitudes do vary and the timing at Island Beach is inconsistent.

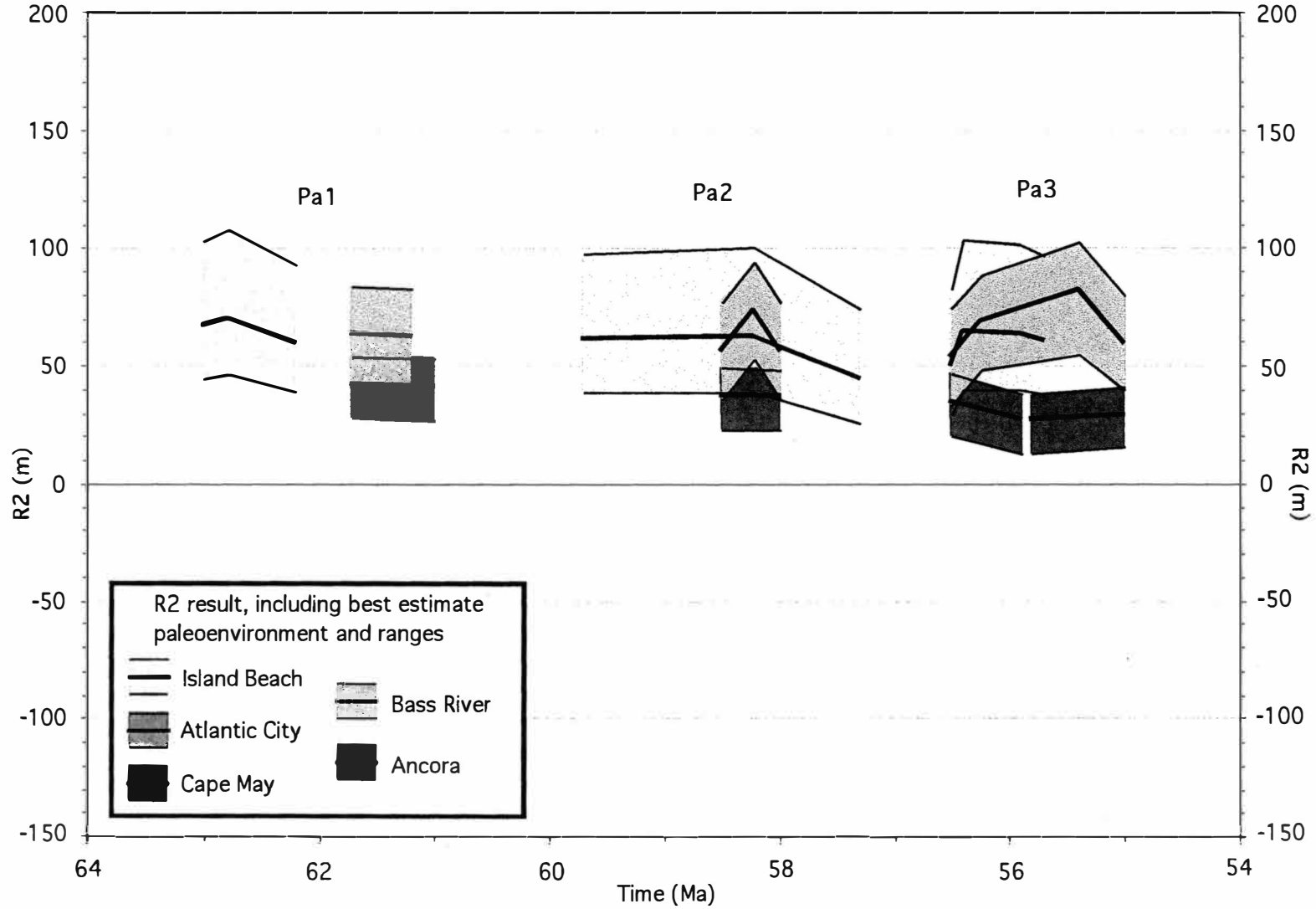

Figure 23. R2 Results for Paleocene Age Sequences.

Deposition at Island Beach should continue during deposition at Bass River and Ancora.

The variation in eustatic amplitudes between early Eocene sequences are small, but show some variability (Figure 24). The maximum variation of R2 between sequences is as much as 30 m, but are generally as low as 10 m. The trends between sequences are quite comparable (assuming best-estimate paleodepths) where they are present in multiple wells with a few exceptions. The offset of sequence E2 at Ancora is most likely due to age uncertainties. Poor fossil preservation occurred in sequence E5 for both boreholes so ages from the Island Beach borehole were used as a reference. Sequence E6a at Bass River was thought to be equivalent to sequence E6 at Ancora. Sequence E6a at Bass River could not be dated using nannofossils due to poor fossil preservation. Therefore, the age of E6a was interpolated from the nearby ACGS#4 borehole (Mays Landing, NJ). At Ancora, the sediments we are calling E6 are younger. Thus, sequence E6a at Bass River represents a separate sequence. Sequence E6 was not preserved at Island Beach and penetration was not sufficiently deep at Atlantic City and Cape May. Ages from the Island Beach borehole were used as references for sequences E7 and E8 due to poor preservation. The variation in the magnitude of R2 across the sequence boundaries are consistent through most of the Eocene, showing a long-term fall in R2 of ≈100 m.

The eustatic amplitudes of Oligocene age sequences (Figure 25) reveal little variation between sequences. The maximum variation in the amplitude of R2 between sequences is 20 m. Only one sequence in the Oligocene is

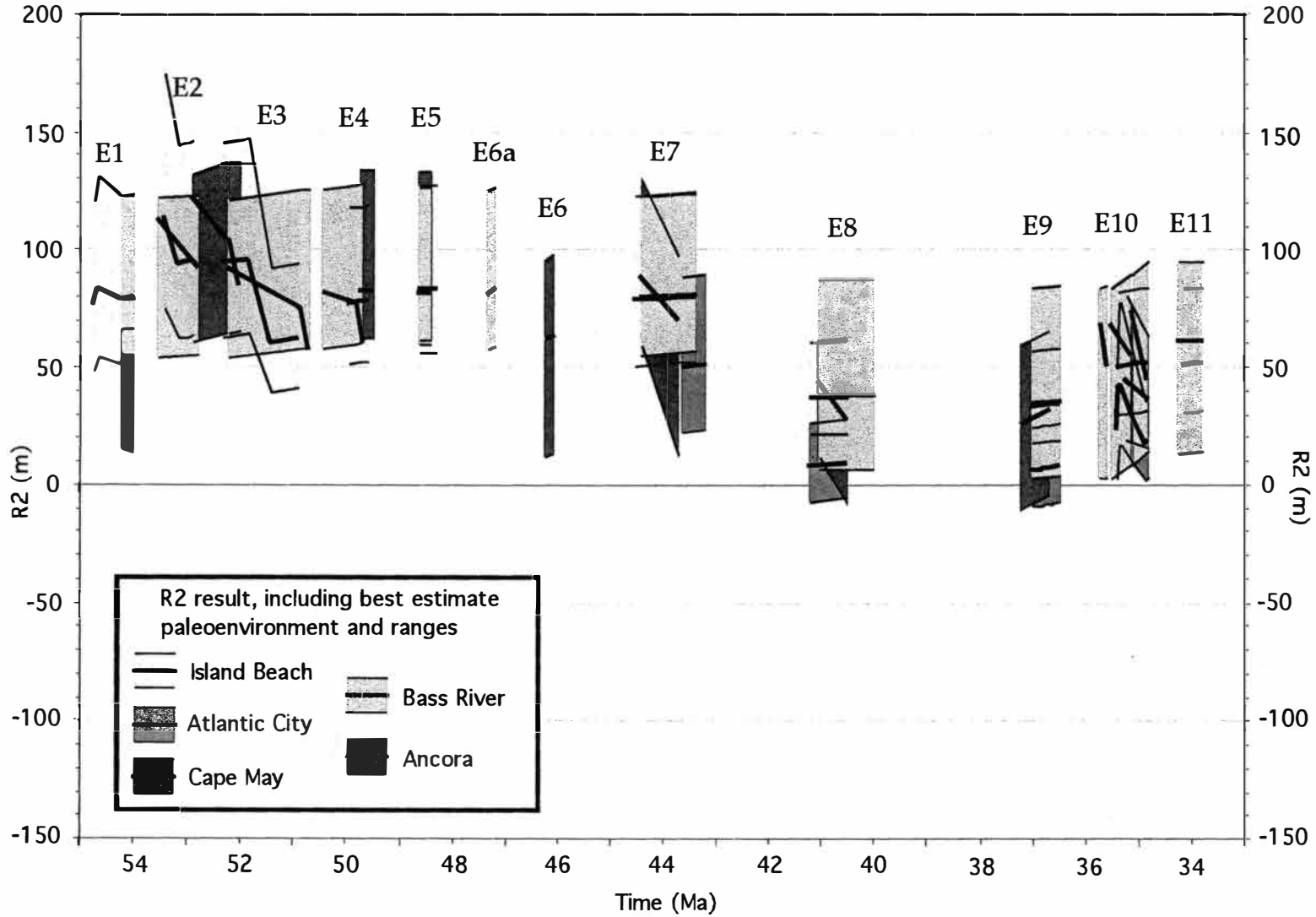

Figure 24. R2 Results for Eocene Age Sequences.

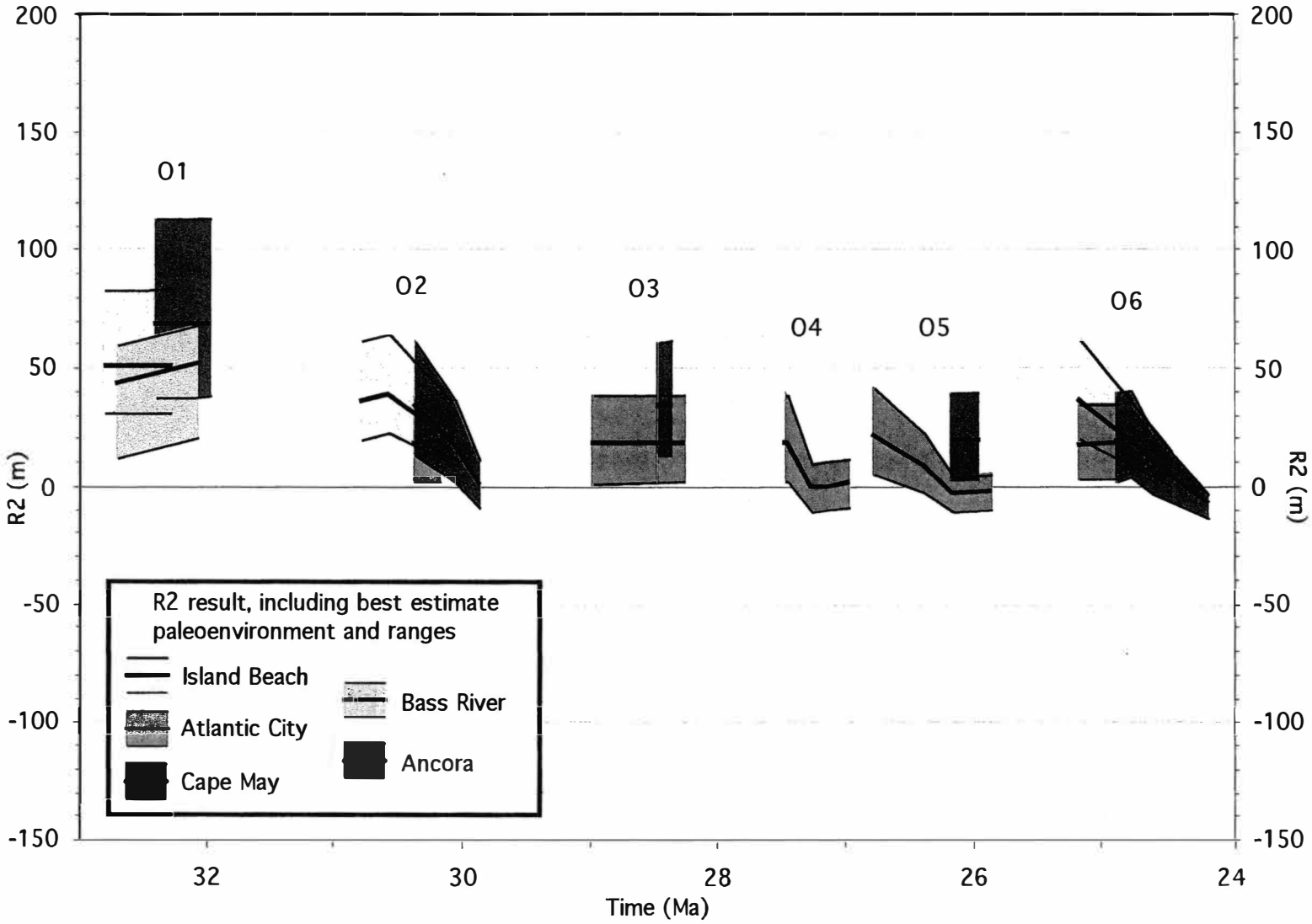

Figure 25. R2 Results for Oligocene Age Sequences.

present in the new boreholes (O1 from Bass River). The magnitude and duration of R2 for O1 (Bass River) is very similar to the other boreholes with a magnitude of about 50 m. Oligocene sequences of the New Jersey margin represent prograding clinoforms across the margin (Figure 12) in response to an increase in terrigenous sediment supply that filled available accommodation. Oligocene clastic progradation is linked with climatic cooling rather than tectonic processes (Steckler et al., 1999).

The amplitudes of R2 for Miocene and younger age sediments (Figure 26) show little variability between sequences, with the exception of Bass River. The magnitudes of R2 at Bass River are consistently about 30 m higher compared to the other boreholes. The timing of R2 is also very inconsistent between boreholes. This is expected for sediments that represent a diversity of paleoenvironments ranging from fluvial to inner neritic. Age constraints are either poor or lacking in shallow-water and non-marine facies.

Although the R2 curves show a similar long-term pattern to the Haq et al. (1987) curve, the magnitudes are substantially lower (Figure 21). The Haq et al. (1987) 3rd order sea-level curve is more readily compared to the R2 curves if it is shifted down 100 m (Figure 21). In general, the best-estimate R2 results yield considerably lower amplitude eustatic variations than the Haq et al. (1987) curve in the Cretaceous. However, there is some similarity in the number and relative duration of their Cretaceous curve and those obtained from the New Jersey data, if allowance is made for the uncertainties in time scales of ± 1 m.y. The best-fit paleodepths correspond well to the Haq et al. (1987) curve in the early Eocene with a falling trend through the middle and

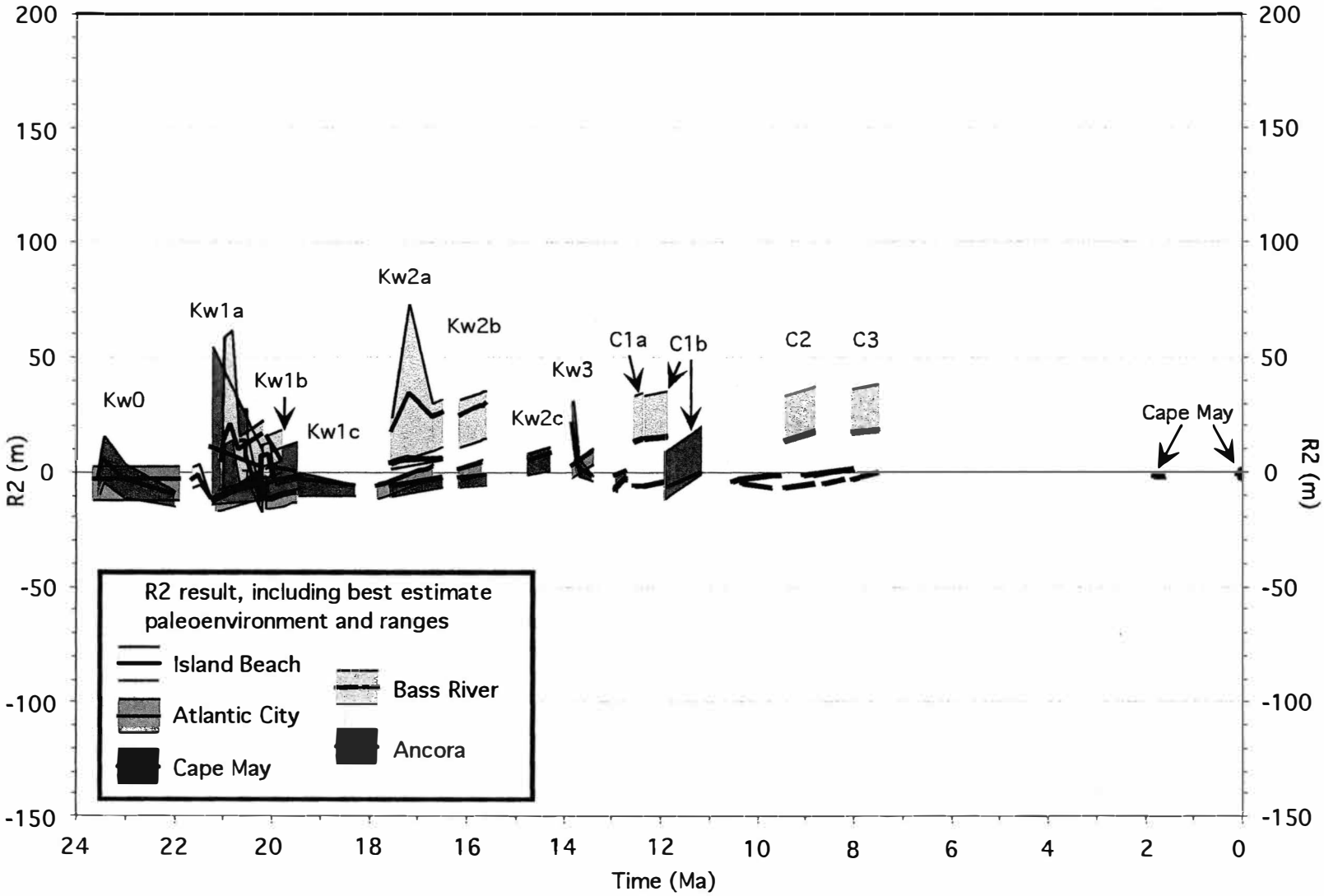

Figure 26. R2 Results for Miocene Through Holocene Age Sequences.

late Eocene. A slight sea level rise in the early Oligocene followed by a fall is observed in both curves. As is the case in the Cretaceous, the eustatic falls of the Haq et al. (1987) curve are much greater. Similar trends and timing for both curves are seen in the Miocene. Again, amplitudes are generally much less in the R2 results.

CHAPTER V

CONCLUSIONS

Additional backstripping analysis of stratigraphic data from the Bass River and Ancora boreholes (ODP Leg 174AX) yield new estimates of magnitudes of R2 in the late Cretaceous. Cenozoic R2 results are consistent with the previous estimates of Kominz et al. (1998). This supports the suggestion that these R2 curves are estimates of eustasy and suggests that the input data, tectonic subsidence assumptions, and backstripping assumptions are correct.

The R2 curves reveal some variability in the amplitudes of 3rd order (0.5 – 3 m.y.) sea-level changes (assuming best-estimate paleodepths), but the best estimate of R2 at Bass River and Ancora do fall well within the ranges of R2 obtained form the other boreholes. Variability in the amplitudes of 3rd order sea-level changes occur in the new Cretaceous eustatic curves which have amplitudes that vary by as much as 50 m (assuming best-estimate paleodepths) both between sequences and across sequence boundaries. This suggests that the maximum amplitude of 3rd order sea-level change was about 90 m if we assume that half of the eustatic signal was captured in sequences lacking lowstand deposits. The Paleocene through early Eocene eustatic amplitudes is also variable between sequences and across sequence boundaries. The maximum 3rd order variations are as much as 90 m across sequence boundaries, but generally are less than 50 m. The middle Eocene

through Oligocene sequences shows as much as 70 m amplitude, but are usually less than 30 m. The eustatic amplitudes are generally less than 20 m in the Miocene, but occasionally are as high as 50 m.

The R2 curves show a similar pattern to the Haq et al. (1987) long-term sea-level curves, but the magnitudes are substantially lower. The R2 curves are comparable to the Haq et al. (1987) 3rd order sea-level curve if it is shifted down 100 m, although magnitudes do vary. Again, it must be noted that only about half of the eustatic signal is assumed to be present in the absence of lowstand deposits. The variation in magnitudes may also be the result of varied rates of sedimentation, local tectonics, or other non-thermal factors. The Cretaceous portion of R2 yields amplitudes that are considerably lower than the Haq et al. (1987) 3rd order curve, although there is a similarity in the number and relative duration of sequences between the two curves. The amplitudes of R2 (assuming best-estimate paleodepths) correspond well to the Haq et al. (1987) curve in the Eocene (with the 100 m drop), but the timing of sequences are inconsistent. The trends are similar in the Oligocene but again the magnitudes vary, especially in regards to the early Oligocene sea-level fall. Comparison of R2 with the Haq et al. (1987) curve of Miocene through Holocene age is difficult due to the presence of shallow to non-marine facies during this time.

Since R2 results are assumed to represent variations in eustatic sea-level change, new porosity-depth relationships from the New Jersey Coastal Plain yield more precise estimates of the magnitude of eustasy. The new porosity data for mud shows an increase in porosity in the upper limit when

compared to curves from the Cost B-2 well. Sand porosity from the coastal plain sediments remains consistent to that at the Cost B-2 well. The upper limit of sand at zero depth remains at 70% while mud increased from 75% to 86%. The new, low porosity data was consistent with Cost B-2 well data so no change was needed for the lower limits. Therefore, the resultant range of porosity for sand at zero depth is 55% to 70% while shale range between 55% to 86%.

This study has enhanced our knowledge and understanding of eustasy through backstripping analysis of additional boreholes drilled recently at Bass River and Ancora. Because they are located in a more up-dip direction, they targeted older sequences (upper Cretaceous). This additional stratigraphic data was necessary to compare with results from Island Beach. It also provided a better estimate of the magnitude of long-term sea-level change and yields new information on older short-term (3rd order) eustatic signals. Results from this study have extended and refined the previously published data of Kominz et al. (1998), further indicating that a eustatic signal can be extracted from stratigraphic data if the input data and assumptions are correct.

Appendix A

Log Data

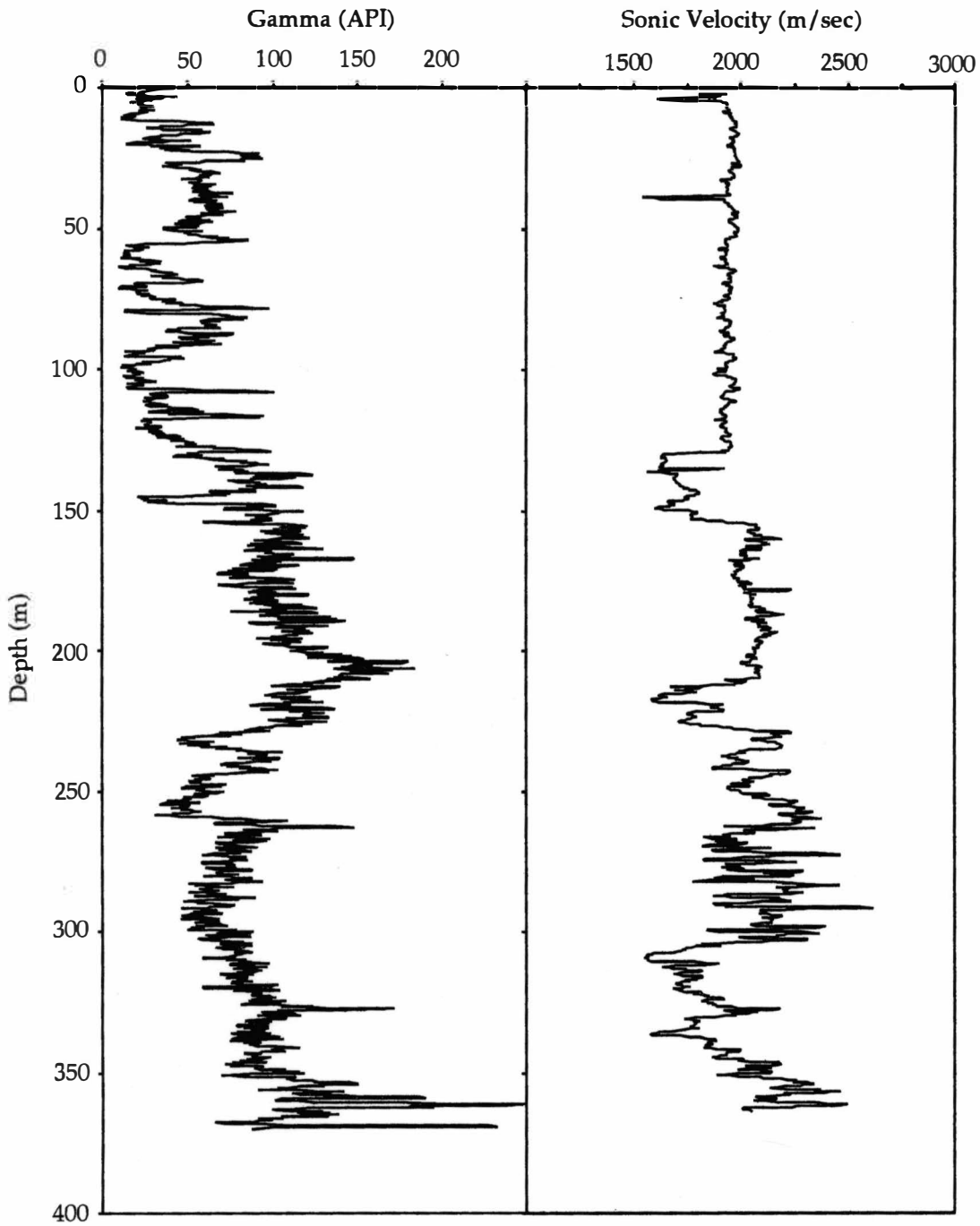

Gamma and sonic data for the Island Beach borehole.

Source: Miller et al. (1994)

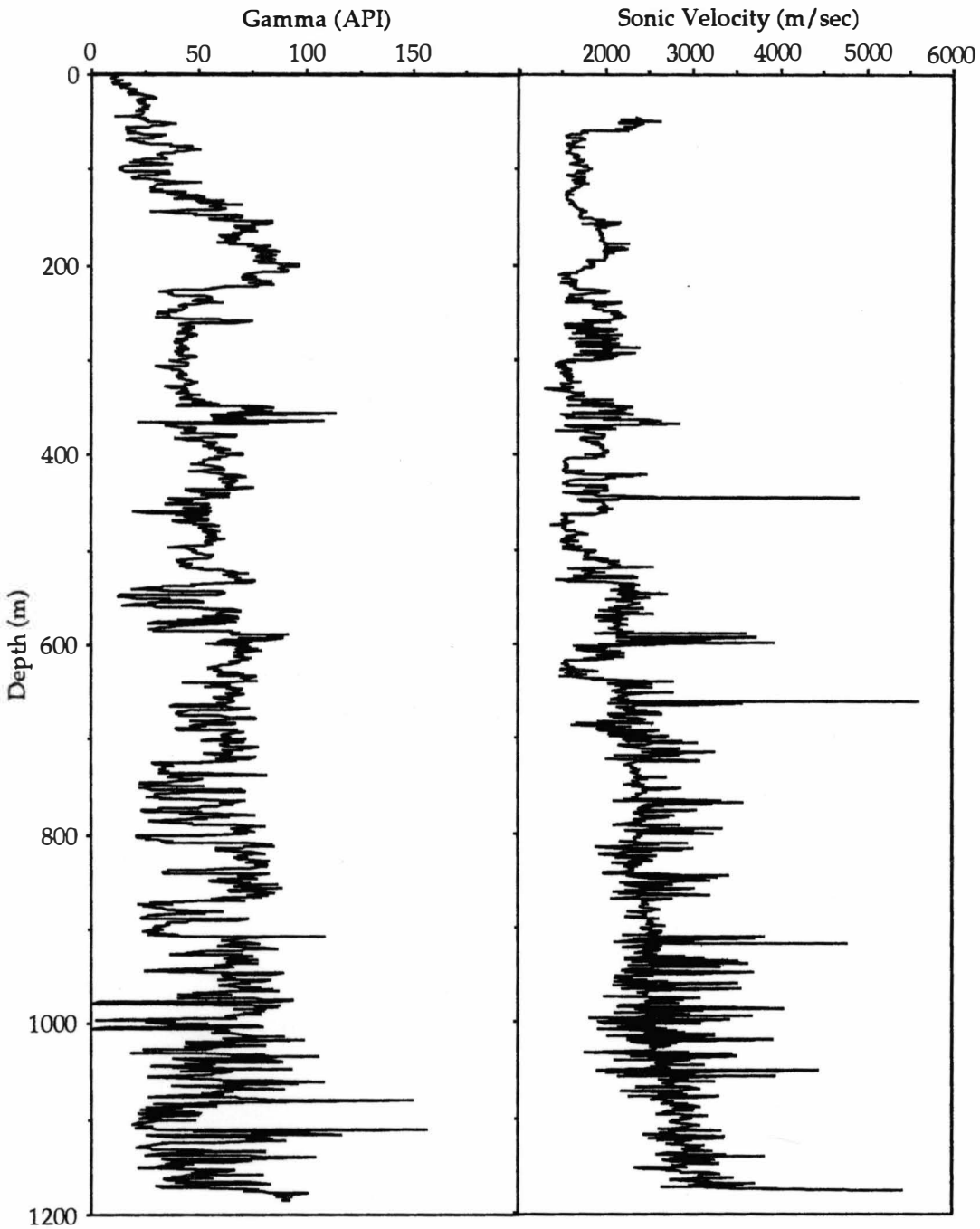

Gamma and sonic data for the Island Beach well #33-01031. Data digitized from analog data.

Source: Analog data provided by Lloyd Mullikin of the New Jersey Geological Survey.

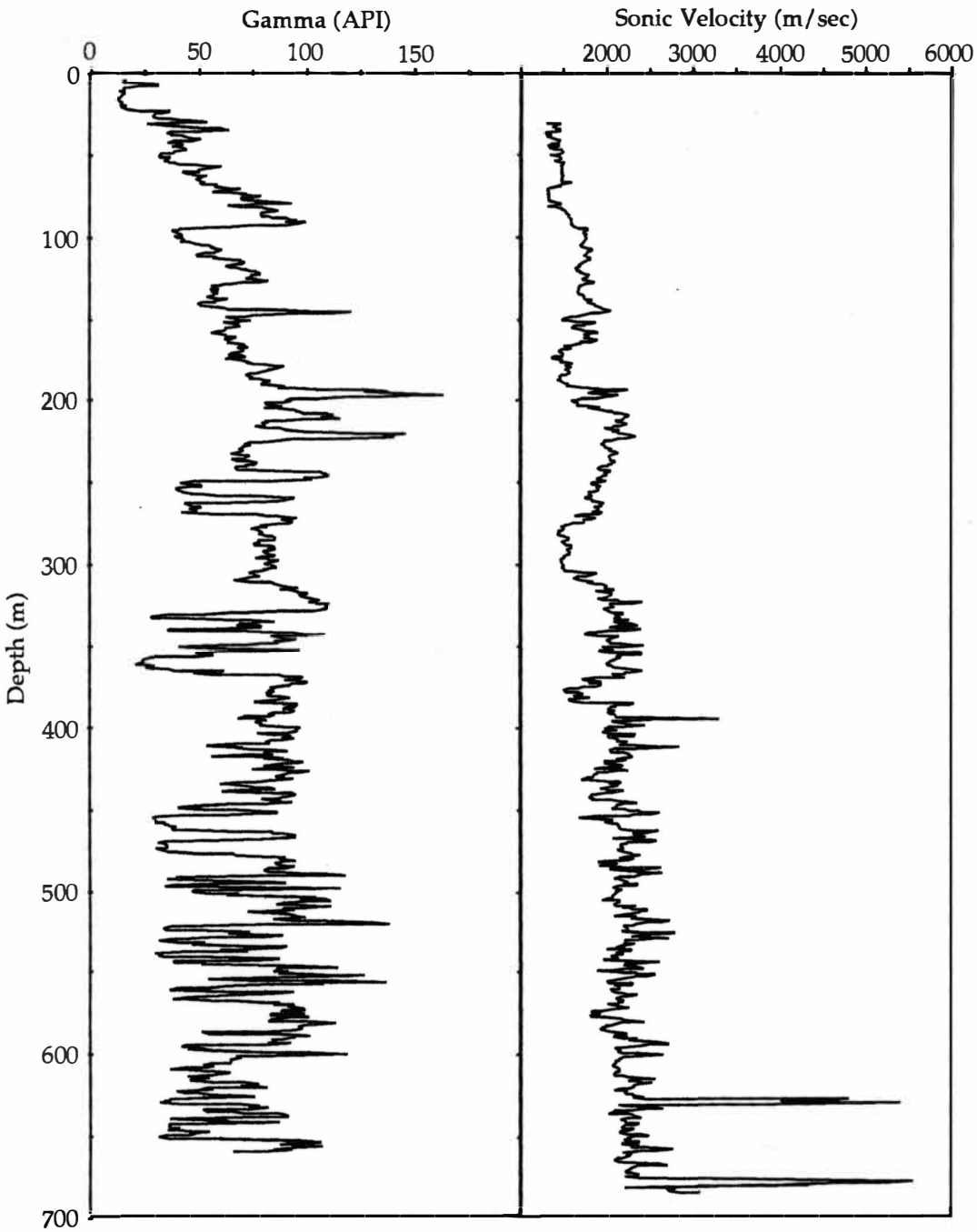

Gamma and sonic data for the Butler Place well. Data digitized from analog data.

Source: Analog data provided by Lloyd Mullikin of the New Jersey Geological Survey.

Appendix B

Lithostratigraphic Data for the Bass River Borehole

Lithostratigraphic Data

Unit	Depth (m) (top of unit)	Density (g/cm^3)	*Age (Ma) (top of unit)	*Paleowater depth (m)		
				Min.	Best	Max.
Poto	616.16	2.6658	95	0	10	30
Unc1	616.15	2.65	94	0	10	30
Bass	596.35	2.6680	—	30	60	100
Bass1	594.37	2.6705	—	30	50	100
Bass2	588.27	2.6725	—	0	40	100
Bass3	574.56	2.6750	—	0	30	100
Bass4	567.24	2.6899	—	0	20	30
Bass5	560.56	2.6834	—	0	20	30
Bass6	556.27	2.6753	—	0	40	100
Bass7	553.25	2.6848	—	0	20	30
Bass8	550.60	2.6731	91.8	0	20	30
Unc2	550.59	2.65	91	0	0	20
Mag1	542.55	2.6859	—	0	0	20
Mag2	534.02	2.6772	90	0	0	0
Unc3	534.01	2.65	87.2	0	0	0
Mag3	527.31	2.6648	—	0	0	0
Mag4	520.97	2.6619	86.8	0	0	30
Unc4	520.96	2.65	85.5	0	20	30
Cheese1	519.42	2.6789	—	0	30	100
Cheese2	513.05	2.6478	85	0	10	30
Unc5	513.04	2.65	84.5	30	100	100
Merch1	509.02	2.6402	—	30	125	150
Merch2	504.45	2.6754	83	30	100	150
Unc6	504.44	2.65	80.5	0	50	100
Wood1	479.76	2.6776	—	0	50	100
Wood2	467.87	2.6775	—	0	20	30
Wood3	453.55	2.6854	—	0	20	30
lEng	448.85	2.6769	76.1	0	20	30
Unc7	448.84	2.65	76	0	20	30
uEng	439.07	2.6639	75	0	20	30

Lithostratgraphic Data—continued

Unc8	439.06	2.65	74.75	30	100	150
Marsh	435.56	2.6436	—	100	120	200
Wenona	423.98	2.6627	—	30	60	100
MtL1	411.18	2.6537	—	0	40	100
MtL2	394.57	2.6486	71.5	0	30	100
Unc9	394.56	2.65	69.3	100	200	200
Nave	389.39	2.6713	—	100	175	200
NewE	383.66	2.6651	64.5	100	150	200
Unc10	383.65	2.65	61.7	75	105	135
Hopa1	382.99	2.6574	61.2	75	105	135
Unc11	382.98	2.65	58.5	75	105	135
Hopa2	380.67	2.6452	—	100	130	160
Vipa2	378.20	2.6668	58	75	105	135
Unc12	378.19	2.65	56.5	75	105	135
Vipa3a	372.77	2.6715	—	95	125	155
Vipa3b	355.10	2.6702	—	100	140	170
Vipa3c	347.05	2.6725	55	75	105	135
Unc13	347.04	2.65	54.14	100	135	200
MnE1	345.83	2.6613	54	100	135	200
Unc14	345.82	2.65	53.5	100	185	200
MnE2	337.87	2.6751	52.8	100	155	200
Unc15	337.86	2.65	52.2	100	155	200
MnE3a	312.42	2.6766	—	100	125	200
MnE3b	309.83	2.6713	50.7	100	100	200
Unc16	309.82	2.65	50.4	100	135	200
MnE4a	299.10	2.6728	49.8	100	125	200
MnE4b	292.58	2.6738	49.7	100	100	200
Unc17	292.57	2.65	48.6	100	135	200
lSRE5	290.90	2.6742	48.4	100	135	200
Unc18	290.89	2.65	47.3	100	135	200
lSRE6a	284.08	2.6753	47.2	100	135	200
Unc19	284.07	2.65	44.4	100	135	200
lSRE7	270	2.6766	43.4	100	135	200

Lithostratigraphic Data—continued

Unc20	269.99	2.65	41	30	75	150
uSRE8	263.23	2.6722	40	30	75	150
Unc21	263.22	2.65	37	30	75	150
uSRE9	258.05	2.6559	36.5	30	75	150
Unc22	258.04	2.65	35.7	30	125	150
AlE10a	256.07	2.6533	35.6	30	100	150
Unc23	256.06	2.65	35.5	30	125	150
AlE10b	234.91	2.6603	35.15	30	100	150
Unc24	234.90	2.65	35.1	30	125	150
AlE10c	208.76	2.6579	34.8	30	75	150
Unc25	208.75	2.65	34.2	30	100	150
AlE11	205.86	2.6701	33.8	30	100	150
Unc26	205.85	2.65	32.7	30	75	100
ACO1	169.26	2.6237	32.1	30	75	100
Unc27	169.25	2.65	21	0	20	30
Kw1a1	166.73	2.6386	—	30	30	100
Kw1a2	157.28	2.6639	—	30	40	100
Kw1a3	148.29	2.6713	—	0	20	30
Kw1a4	116.74	2.6558	20.2	0	20	30
Unc28	116.73	2.65	20.1	0	20	20
Kw1b	100.28	2.6575	19.8	0	0	20
Unc29	100.27	2.65	17.5	0	20	30
Kw2a1	88.06	2.6605	—	0	40	100
Kw2a2	70.84	2.6704	—	0	20	30
Kw2a3	62.48	2.6575	16.5	0	20	30
Unc30	62.47	2.65	16.1	0	20	30
Kw2b1	50.90	2.6613	—	0	20	30
Kw2b2	45.54	2.6706	—	0	20	30
Kw2b3	42.98	2.6620	—	0	20	30
Kw2b4	40.51	2.6688	15.6	0	20	30
Unc31	40.50	2.65	12.5	0	0	30
C1a	37.80	2.6569	12.4	0	0	30
Unc32	37.79	2.65	12.3	0	0	30

Lithostratigraphic Data—continued

C1b	31.06	2.6570	11.9	0	0	30
Unc33	31.05	2.65	9.4	0	0	30
C2	12.44	2.6579	8.8	0	0	30
Unc34	12.43	2.65	8	0	0	30
C3	6	2.6605	7.5	0	0	30
Unc35	5.99	2.65	.011	0	0	0
CapeM	0	2.6545	0	0	0	0

* Data provided by Ken Miller [1], Richard Olsson [1], Steve Pekar [1], Ben Cramer [1], and Jim Browning [2] (Rutgers University [1], University of North Carolina [2]).

Cumulative Percent of Lithologies

Unit	Cumulative Percent					
	Clay	Sand	Glauconite	Forams	Mica	Other
Poto	70	30	0	0	0	0
Unc1	0	0	0	0	0	0
Bass	80	20	0	0	0	0
Bass1	95	1.0	3.0	1.0	0	0
Bass2	100	0	0	0	0	0
Bass3	97.4	0	0	0.9	1.7	0
Bass4	75	6.7	0	5.0	13.3	0
Bass5	78.2	9.1	0	3.6	9.1	0
Bass6	97.1	0.6	0	0	2.3	0
Bass7	88	2.0	0	0	10	0
Bass8	76.7	18.7	0	1.3	3.3	0
Unc2	0	0	0	0	0	0
Mag1	80.2	7.9	0	0	11.9	0
Mag2	32.5	54.3	0	0	13.2	0
Unc3	0	0	0	0	0	0
Mag3	65.5	34.5	0	0	0	0
Mag4	53.1	46.9	0	0	0	0
Unc4	0	0	0	0	0	0

Cumulative Percent of Lithologies —continued

Cheese1	88.6	0.7	3.6	0	7.1	0
Cheese2	45.8	29.2	25	0	0	0
Unc5	0	0	0	0	0	0
Merch1	53.8	2.5	43.7	0	0	0
Merch2	81.3	0	3.7	15	0	0
Unc6	0	0	0	0	0	0
Wood1	95.2	0	0.5	0	4.3	0
Wood2	86.9	7.3	0.4	0	5.4	0
Wood3	71.1	15.9	0	0	13	0
lEng	47.5	35	5.0	0	12.5	0
Unc7	0	0	0	0	0	0
uEng	51.7	30.5	12.2	0	5.6	0
Unc8	0	0	0	0	0	0
Marsh	49.6	6.4	40	4.0	0	0
Wenona	55.5	36.7	5.8	0	2.0	0
MtL1	35.8	55.4	8.8	0	0	0
MtL2	27.9	56.7	15.4	0	0	0
Unc9	0	0	0	0	0	0
Nave	58.5	5.0	12.5	24	0	0
NewE	76.2	0.9	14.3	8.6	0	0
Unc10	0	0	0	0	0	0
Hopa1	59.1	9.1	22.7	9.1	0	0
Unc11	0	0	0	0	0	0
Hopa2	35	22	35	8.0	0	0
Vipa2	70	10	10	10	0	0
Unc12	0	0	0	0	0	0
Vipa3a	80	5.0	5.0	10	0	0
Vipa3b	93.9	2.7	2.7	0.7	0	0
Vipa3c	100	0	0	0	0	0
Unc13	0	0	0	0	0	0
MnE1	77.8	0	17.8	4.4	0	0
Unc14	0	0	0	0	0	0
MnE2	89.4	1.2	0.6	8.8	0	0

Cumulative Percent of Lithologies —continued

Unc15	0	0	0	0	0	0
MnE3a	88.2	0.5	0	11.2	0	0
MnE3b	74.1	14.8	1.8	9.3	0	0
Unc16	0	0	0	0	0	0
MnE4a	99.1	0	0	0.9	0	0
MnE4b	92.4	1.4	0.7	5.5	0	0
Unc17	0	0	0	0	0	0
lSRE5	95.6	0	0	4.4	0	0
Unc18	0	0	0	0	0	0
lSRE6a	88.7	0	1.3	10	0	0
Unc19	0	0	0	0	0	0
lSRE7	84.1	2.0	0.6	13.3	0	0
Unc20	0	0	0	0	0	0
uSRE8	68.7	6.3	7.5	17.5	0	0
Unc21	0	0	0	0	0	0
uSRE9	56.4	14.3	22.1	7.2	0	0
Unc22	0	0	0	0	0	0
AlE10a	70	5.0	25	0	0	0
Unc23	0	0	0	0	0	0
AlE10b	78.7	6.6	14.7	0	0	0
Unc24	0	0	0	0	0	0
AlE10c	73.9	8.6	17.5	0	0	0
Unc25	0	0	0	0	0	0
AlE11	95	2.5	2.5	0	0	0
Unc26	0	0	0	0	0	0
ACO1	22.8	14.4	62.8	0	0	0
Unc27	0	0	0	0	0	0
Kw1a1	38	22	40	0	0	0
Kw1a2	61.7	38.3	0	0	0	0
Kw1a3	94.5	5.5	0	0	0	0
Kw1a4	25.8	74.2	0	0	0	0
Unc28	0	0	0	0	0	0
Kw1b	33.1	66.9	0	0	0	0

Cumulative Percent of Lithologies —continued

Unc29	0	0	0	0	0	0
Kw2a1	46.5	53.5	0	0	0	0
Kw2a2	90.6	9.4	0	0	0	0
Kw2a3	33.3	66.7	0	0	0	0
Unc30	0	0	0	0	0	0
Kw2b1	50	50	0	0	0	0
Kw2b2	91.7	8.3	0	0	0	0
Kw2b3	53.3	46.7	0	0	0	0
Kw2b4	83.3	16.7	0	0	0	0
Unc31	0	0	0	0	0	0
C1a	30.8	69.2	0	0	0	0
Unc32	0	0	0	0	0	0
C1b	31	69	0	0	0	0
Unc33	0	0	0	0	0	0
C2	35.1	64.9	0	0	0	0
Unc34	0	0	0	0	0	0
C3	46.8	53.2	0	0	0	0
Unc35	0	0	0	0	0	0
CapeM	20	80	0	0	0	0

Source: Data adapted from Miller et al. (1998).

Percentage of Lithologies Used for Delithification

Unit	Percent Lithology					
	Shale	Micrite	Sandstone	Calcarenite	Siltstone	Calcisiltite
Poto	56	0	30	0	14	0
Unc1	0	0	0	0	0	0
Bass	64	0	20	0	16	0
Bass1	76	0	4.0	1.0	19	0
Bass2	80	0	0	0	20	0
Bass3	77.9	0	1.7	0.9	19.5	0
Bass4	60	0	20	5.0	15	0

Percentage of Lithologies Used for Delithification—continued

Bass5	62.6	0	18.2	3.6	15.6	0
Bass6	77.7	0	2.9	0	19.4	0
Bass7	70.4	0	12	0	17.6	0
Bass8	61.4	0	22	1.3	15.3	0
Unc2	0	0	0	0	0	0
Mag1	64.1	0	19.9	0	16	0
Mag2	26	0	67.5	0	6.5	0
Unc3	0	0	0	0	0	0
Mag3	52.4	0	34.5	0	13.1	0
Mag4	42.5	0	46.9	0	10.6	0
Unc4	0	0	0	0	0	0
Cheese1	70.9	0	11.4	0	17.7	0
Cheese2	36.7	0	54.2	0	9.1	0
Unc5	0	0	0	0	0	0
Merch1	43	0	46.3	0	10.7	0
Merch2	65	0	3.8	15	16.2	0
Unc6	0	0	0	0	0	0
Wood1	76.2	0	4.8	0	19	0
Wood2	69.4	0	13.2	0	17.4	0
Wood3	56.9	0	28.9	0	14.2	0
lEng	38	0	52.5	0	9.5	0
Unc7	0	0	0	0	0	0
uEng	41.4	0	48.3	0	10.3	0
Unc8	0	0	0	0	0	0
Marsh	39.7	0	46.4	4.0	9.9	0
Wenona	44.4	0	44.5	0	11.1	0
MtL1	28.6	0	64.2	0	7.2	0
MtL2	22.3	0	72.1	0	5.6	0
Unc9	0	0	0	0	0	0
Nave	46.8	0	17.5	24	11.7	0
NewE	61	0	15.2	8.6	15.2	0
Unc10	0	0	0	0	0	0
Hopa1	47.3	0	31.8	9.1	11.8	0

Percentage of Lithologies Used for Delithification—continued

Unc11	0	0	0	0	0	0
Hopa2	28	0	57	8.0	7.0	0
Vipa2	56	0	20	10	14	0
Unc12	0	0	0	0	0	0
Vipa3a	64	0	10	10	16	0
Vipa3b	75.2	0	5.3	0.7	18.8	0
Vipa3c	80	0	0	0	20	0
Unc13	0	0	0	0	0	0
MnE1	62.2	0	17.8	4.4	15.6	0
Unc14	0	0	0	0	0	0
MnE2	71.5	0	1.8	8.8	17.9	0
Unc15	0	0	0	0	0	0
MnE3a	70.6	0	0.5	11.2	17.7	0
MnE3b	59.2	0	16.7	9.3	14.8	0
Unc16	0	0	0	0	0	0
MnE4a	79.3	0	0	0.9	19.8	0
MnE4b	73.9	0	2.1	5.5	18.5	0
Unc17	0	0	0	0	0	0
lSRE5	76.4	0	0	4.5	19.1	0
Unc18	0	0	0	0	0	0
lSRE6a	70.9	0	1.3	10	17.8	0
Unc19	0	0	0	0	0	0
lSRE7	67.3	0	2.6	13.3	16.8	0
Unc20	0	0	0	0	0	0
uSRE8	55	0	13.8	17.5	13.7	0
Unc21	0	0	0	0	0	0
uSRE9	45.1	0	36.5	7.1	11.3	0
Unc22	0	0	0	0	0	0
AlE10a	56	0	30	0	14	0
Unc23	0	0	0	0	0	0
AlE10b	62.9	0	21.4	0	15.7	0
Unc24	0	0	0	0	0	0

Percentage of Lithologies Used for Delithification—continued

AlE10c	59.1	0	26.1	0	14.8	0
Unc25	0	0	0	0	0	0
AlE11	76	0	5.0	0	19	0
Unc26	0	0	0	0	0	0
ACO1	18.3	0	77.2	0	4.5	0
Unc27	0	0	0	0	0	0
Kw1a1	30.4	0	62	0	7.6	0
Kw1a2	49.4	0	38.3	0	12.3	0
Kw1a3	75.6	0	5.5	0	18.9	0
Kw1a4	20.7	0	74.2	0	5.1	0
Unc28	0	0	0	0	0	0
Kw1b	26.5	0	66.9	0	6.6	0
Unc29	0	0	0	0	0	0
Kw2a1	37.2	0	53.5	0	9.3	0
Kw2a2	72.5	0	9.4	0	18.1	0
Kw2a3	26.7	0	66.7	0	6.6	0
Unc30	0	0	0	0	0	0
Kw2b1	40	0	50	0	10	0
Kw2b2	73.3	0	8.4	0	18.3	0
Kw2b3	42.7	0	46.7	0	10.6	0
Kw2b4	66.7	0	16.7	0	16.6	0
Unc31	0	0	0	0	0	0
C1a	24.6	0	69.2	0	6.2	0
Unc32	0	0	0	0	0	0
C1b	24.8	0	69	0	6.2	0
Unc33	0	0	0	0	0	0
C2	28.1	0	64.9	0	7.0	0
Unc34	0	0	0	0	0	0
C3	37.4	0	53.2	0	9.4	0
Unc35	0	0	0	0	0	0
CapeM	16	0	80	0	4.0	0

Appendix C

Lithostratigraphic Data for the Ancora Borehole

Lithostratigraphic Data

Unit	Depth (m) (top of unit)	Density (g/cm^3)	*Age (Ma) (top of unit)	*Paleowater depth (m)		
				Min.	Best	Max.
Poto	356.62	2.6658	96.36	0	0	10
Poto1	353.02	2.6709	96	0	0	10
Unc1	353.01	2.65	95.113	0	20	30
Poto2	351.90	2.6750	95	0	20	30
Unc2	351.89	2.65	94.195	0	0	10
Poto3	349.95	2.6722	94	0	0	10
Unc3	349.94	2.65	93.25	30	50	100
Bass1	342.90	2.6828	—	30	40	100
Bass2	340.16	2.6749	—	0	30	100
Bass3	338.61	2.6725	93	0	10	30
Unc4	338.60	2.65	91.2	0	40	100
Bass4	329.95	2.6735	91	0	10	30
Unc5	329.94	2.65	90.45	0	30	100
Bass5	323.85	2.6795	90.3	0	10	30
Unc6	323.84	2.65	88	0	0	20
Mag1	300.84	2.6525	—	0	0	0
Mag2	295.66	2.6651	—	0	0	0
Mag3	291.82	2.6545	87	0	0	0
Unc7	291.81	2.65	85	0	25	40
Cheese	288.13	2.6514	84.9	0	20	30
Unc8	288.12	2.65	81.7	0	50	100
Merch	275.24	2.6314	80.3	30	70	100
Wood	242.99	2.6776	76.4	0	40	100
lEng	241.50	2.6541	76.2	0	20	30
Unc9	241.49	2.65	76	0	40	100
uEng1	234.70	2.6612	—	0	20	30
uEng2	230.80	2.6550	75	0	10	30
Unc10	230.79	2.65	74.9	0	30	100
Marsh	224.03	2.6457	74.5	0	50	100
Wenona	218.85	2.6549	73.5	0	30	100
MtL	198.52	2.6476	71.5	0	20	30

Lithostratigraphic Data —continued

Unc11	198.51	2.65	66.5	0	60	100
NavHo1	186.69	2.6349	64.4	0	50	100
Unc12	186.68	2.65	61.7	45	60	75
Hopa1	184.86	2.6565	61	45	60	75
Unc13	184.85	2.65	58.5	45	60	75
Vipa2	182.58	2.6451	58	45	60	75
Unc14	182.57	2.65	56.5	30	60	75
Vipa3a	171.33	2.6597	56.9	30	45	60
Unc15	171.32	2.65	55.8	30	45	60
Vipa3b	159.17	2.6694	55	30	45	60
Unc16	159.16	2.65	54.17	30	70	100
MnE1	158.25	2.6414	54	30	70	100
Unc17	158.24	2.65	52.85	100	185	200
MnE2	140.58	2.6698	52.25	100	155	200
Unc18	140.57	2.65	52.2	100	155	200
MnE3	136.77	2.6708	52	100	125	200
Unc19	136.76	2.65	49.7	100	125	200
lSRE4	136.16	2.6687	49.5	100	125	200
Unc20	136.15	2.65	48.6	100	125	200
lSRE5	135.03	2.6399	48.4	100	125	200
Unc21	135.02	2.65	46.2	30	100	150
lSRE6	130.33	2.6657	46.1	30	100	150
Unc22	130.32	2.65	44.4	100	140	200
lSRE7	118.45	2.6718	43.7	30	110	150
Unc23	118.44	2.65	41	30	75	100
uSRE8	109.67	2.6537	40.5	0	50	100
Unc24	109.66	2.65	37.2	0	50	100
uSRE9	80.38	2.6654	36.7	0	50	100
Unc25	80.37	2.65	21.2	0	35	100
Kw1a	69.25	2.6614	20.2	0	20	30
Unc26	69.24	2.65	20	0	20	30
Kw1b	51.18	2.6618	19.5	0	10	30
Unc27	51.17	2.65	11.9	0	5	30

Lithostratigraphic Data —continued

C1b	8.92	2.6512	11.2	0	0	30
Unc28	8.91	2.65	8.8	0	0	0
C2	2.74	2.6513	8.3	0	0	0
Surf	0	2.6515	0	0	0	0

* Data provided by Ken Miller [1], Richard Olsson [1], Steve Pekar [1], Ben Cramer [1], and Jim Browning [2] (Rutgers University [1], University of North Carolina [2]).

Cumulative Percent of Lithologies

Unit	Cumulative Percent					
	Clay	Sand	Glauconite	Forams	Mica	Other
Poto	70	30	0	0	0	0
Poto1	90.5	8.6	0.9	0	0	0
Unc1	0	0	0	0	0	0
Poto2	93.3	0	0	6.7	0	0
Unc2	0	0	0	0	0	0
Poto3	87.5	8.3	0	4.2	0	0
Unc3	0	0	0	0	0	0
Bass1	82.4	8.1	0	0	9.5	0
Bass2	57.4	10	8.0	23.3	1.3	0
Bass3	100	0	0	0	0	0
Unc4	0	0	0	0	0	0
Bass4	59.8	30.6	2.2	0	7.4	0
Unc5	0	0	0	0	0	0
Bass5	68.1	16.7	0	9.7	5.5	0
Unc6	0	0	0	0	0	0
Mag1	11.1	88.9	0	0	0	0
Mag2	67.2	32.8	0	0	0	0
Mag3	20	80	0	0	0	0
Unc7	0	0	0	0	0	0
Cheese	31.4	57.1	11.4	0	0	0
Unc8	0	0	0	0	0	0

Cumulative Percent of Lithologies —continued

Merch	39.1	1.9	57.1	1.9	0	0
Wood	91.6	1.5	1.3	0.8	4.8	0
lEng	45.8	25	25	0	4.2	0
Unc9	0	0	0	0	0	0
uEng1	59	8.2	25.6	0	7.2	0
uEng2	25	67.1	6.2	0	1.7	0
Unc10	0	0	0	0	0	0
Marsh	40.5	22.6	33.3	2.4	1.2	0
Wenona	41.7	38.3	15	5.0	0	0
MtL	26.1	57.2	16.7	0	0	0
Unc11	0	0	0	0	0	0
NavHo1	36.1	5.3	53	5.6	0	0
Unc12	0	0	0	0	0	0
Hopa1	25	25	33.3	8.4	8.3	0
Unc13	0	0	0	0	0	0
Vipa2	20.8	25	41.7	8.3	4.2	0
Unc14	0	0	0	0	0	0
Vipa3a	62.4	16.7	16.8	2.3	1.8	0
Unc15	0	0	0	0	0	0
Vipa3b	90.7	3.7	4.0	1.6	0	0
Unc16	0	0	0	0	0	0
MnE1	40	16	40	4.0	0	0
Unc17	0	0	0	0	0	0
MnE2	87	9.0	2.0	2.0	0	0
Unc18	0	0	0	0	0	0
MnE3	86	8.0	2.0	4.0	0	0
Unc19	0	0	0	0	0	0
lSRE4	80	6.7	6.7	6.6	0	0
Unc20	0	0	0	0	0	0
lSRE5	42	10	44	4.0	0	0
Unc21	0	0	0	0	0	0
lSRE6	68	6.4	13.6	12	0	0

Cumulative Percent of Lithologies —continued

Unc22	0	0	0	0	0	0
lSRE7	77.2	9.1	3.4	10.3	0	0
Unc23	0	0	0	0	0	0
uSRE8	52.8	16.8	24	6.4	0	0
Unc24	0	0	0	0	0	0
uSRE9	20	57.7	2.3	20	0	0
Unc25	0	0	0	0	0	0
Kw1a	50.8	49.2	0	0	0	0
Unc26	0	0	0	0	0	0
Kw1b	52.6	47.4	0	0	0	0
Unc27	0	0	0	0	0	0
C1b	5.2	94.8	0	0	0	0
Unc28	0	0	0	0	0	0
C2	5.7	94.3	0	0	0	0
Surf	6.7	93.3	0	0	0	0

Source: Data adapted from Miller et al. (1999).

Percentage of Lithologies Used for Delithification

Unit	Percent Lithology					
	Shale	Micrite	Sandstone	Calcarenite	Siltstone	Calcisiltite
Poto	56	0	30	0	14	0
Poto1	72.4	0	8.6	0.9	18.1	0
Unc1	0	0	0	0	0	0
Poto2	74.7	0	0	6.7	18.6	0
Unc2	0	0	0	0	0	0
Poto3	70	0	8.3	4.2	17.5	0
Unc3	0	0	0	0	0	0
Bass1	65.9	0	17.6	0	16.5	0
Bass2	45.9	0	19.3	23.3	11.5	0
Bass3	80	0	0	0	20	0

Percentage of Lithologies Used for Delithification —continued

Unc4	0	0	0	0	0	0
Bass4	47.8	0	40.2	0	12	0
Unc5	0	0	0	0	0	0
Bass5	54.5	0	22.2	9.7	13.6	0
Unc6	0	0	0	0	0	0
Mag1	8.9	0	88.9	0	2.2	0
Mag2	53.8	0	32.8	0	13.4	0
Mag3	16	0	80	0	4.0	0
Unc7	0	0	0	0	0	0
Cheese	25.1	0	68.6	0	6.3	0
Unc8	0	0	0	0	0	0
Merch	31.2	0	59.1	1.9	7.8	0
Wood	73.3	0	7.6	0.8	18.3	0
lEng	36.7	0	54.2	0	9.1	0
Unc9	0	0	0	0	0	0
uEng1	47.2	0	41	0	11.8	0
uEng2	20	0	75	0	5.0	0
Unc10	0	0	0	0	0	0
Marsh	32.4	0	57.1	2.4	8.1	0
Wenona	33.3	0	53.3	5.0	8.4	0
MtL	20.9	0	73.9	0	5.2	0
Unc11	0	0	0	0	0	0
NavHo1	28.9	0	58.3	5.6	7.2	0
Unc12	0	0	0	0	0	0
Hopa1	20	0	66.7	8.3	5.0	0
Unc13	0	0	0	0	0	0
Vipa2	16.7	0	70.8	8.3	4.2	0
Unc14	0	0	0	0	0	0
Vipa3a	49.9	0	35.3	2.3	12.5	0
Unc15	0	0	0	0	0	0
Vipa3b	72.5	0	7.8	1.6	18.1	0
Unc16	0	0	0	0	0	0
MnE1	32	0	56	4.0	8.0	0

Percentage of Lithologies Used for Delithification —continued

Unc17	0	0	0	0	0	0
MnE2	69.6	0	11	2.0	17.4	0
Unc18	0	0	0	0	0	0
MnE3	68.8	0	10	4.0	17.2	0
Unc19	0	0	0	0	0	0
lSRE4	64	0	13.3	6.7	16	0
Unc20	0	0	0	0	0	0
lSRE5	33.6	0	54	4.0	8.4	0
Unc21	0	0	0	0	0	0
lSRE6	54.4	0	20	12	13.6	0
Unc22	0	0	0	0	0	0
lSRE7	61.7	0	12.6	10.3	15.4	0
Unc23	0	0	0	0	0	0
uSRE8	42.2	0	40.8	6.4	10.6	0
Unc24	0	0	0	0	0	0
uSRE9	16	0	60	20	4.0	0
Unc25	0	0	0	0	0	0
Kw1a	40.6	0	49.2	0	10.2	0
Unc26	0	0	0	0	0	0
Kw1b	42.1	0	47.4	0	10.5	0
Unc27	0	0	0	0	0	0
C1b	4.2	0	94.8	0	1.0	0
Unc28	0	0	0	0	0	0
C2	4.6	0	94.3	0	1.1	0
Surf	5.3	0	93.4	0	1.3	0

REFERENCES CITED

Anselmetti, F.S., and Eberli, G.P., 1999, The velocity-deviation log: A tool to Predict pore type and permeability trends in carbonate drill holes from Sonic and porosity or density logs: AAPG Bulletin, v.83, n.3, p.450-466.

Asquith, G.B., and Gibson, C.R., 1982, Basic Well Log Analysis for Geologists: AAPG Methods in Exploration Series, n.3, 216 p.

Berggren, W.A., Kent, D.V., Swisher III, C.C., and Aubry, M.P., 1995, A revised Cenozoic geochronology and chronostratigraphy, *in* Berggren, W.A., Kent, D.V., Aubry, M.P., and Hardenbol, J.G., eds., Geochronology, Time Scales and Global Stratigraphic Correlation: SEPM Special Publication, n.54, p.129–212.

Bond, G.C., and Kominz, M.A., 1984, Construction of tectonic subsidence curves for the early Paleozoic miogeocline, southern Canadian Rocky Mountains: Implications for the subsidence mechanisms, age of breakup, and crustal thinning: Geological Society of America Bulletin, v.95, p.155-173.

Bond, G.C., Kominz, M.A., Steckler, M.S., and Grotzinger, J.P., 1989, Role of thermal subsidence, flexure and eustasy in the evolution of early Paleozoic passive-margin carbonate platforms, *in* Crevello, P.D., Wilson, J.L., Sarg, J.F., and Read, J.F., eds., Controls on carbonate platform and basin development: SEPM (Society for Sedimentary Geology) Special Publication 44, p.39-61.

Bond, G.C., and, Kominz, M.A., 1991, Disentangling middle Paleozoic sea level and tectonic events in cratonic margins and cratonic basins of North America: Journal of Geophysical Research, v.96, p.6619-6639.

Emery, D., and Myers, K.J., eds., 1996, Sequence Stratigraphy: Uxbridge, London, 297 p.

Erickson, S.N., and Jarrard, R.D., 1998, Velocity-porosity relationships for water-saturated siliciclastic sediments: Journal of Geophysical Research, v.103, n.B12, p.30,385 -30,406.

Gill, H.E., Seaber, P.R., Vecchioli, J., and Anderson, H.R., 1963, Evaluation of The geologic and hydrologic data from the test-drilling program at Island Beach State Park, N.J.: State of New Jersey, Dept. of Conservation And Economic Development, Div. Of Water Policy and Supply, Water Resources Circular, n.12, 25 p.

Gradstein, F.M., Agterberg, F.P., Ogg, J.G., Hardenbol, J., Van Veen, P., Thierry, J., and Huang, Z., 1995, A Triassic, Jurassic and Cretaceous time scale, *in* Berggren, W.A., Kent, D.V., Aubry, M.P., and Hardenbol, J.G., eds., Geochronology, Time Scales and Global Stratigraphic Correlation: SEPM Special Publication, n.54, p. 95-126.

Grow, J.A., and Sheridan, R.E., 1988, U.S. Atlantic Cotinental Margin: A typical Atlantic-type or passive continental margin, *in* Sheridan, R.E., and Grow, J.A., eds., The Atlantic Continental Margin, U.S.,: Geological Society of America, The Geology of North America, v.1-2, p. 1-7.

Haq, B.U., Hardenbol, J., and Vail, P.R., 1987, Chronology of fluctuating sea levels since the Triassic (250 million years ago to present): Science, v.235, p.1156-1167.

Jervey, M.T., 1988, Quantitative geological modeling of siliciclastic rock sequences and their seismic expressions, *in* Wilgus, C.K., Hastings, B.S., St.Kendall, C.G., Posamentier, H.W., Ross, C.A., and Van Wagoner, J.C., Sea-level changes: An integrated approach, SEPM Special Publication 42, p.47-69.

Kendall, C.G.St.C., Moore, P., Whittle, G., and Cannon, R., 1992, A challenge: Is it possible to determine eustasy and does it matter?, *in* Dott, R.H., Jr., ed., Eustasy: The Historical Ups and Downs of a Major Geological Concept: GSA Memoir, n.180, 111 p.

Klitgord, K.D., Hutchinson, D.R., and Schouten, H., 1988, U.S. Atlantic Continental margin; Structural and tectonic framework, *in* Sheridan, R.E., and Grow, J.A., eds., The Atlantic Continental Margin, U.S.: Geological Society of America, The Geology of North America, v. 1-2, p.19-55.

Kominz, M.A., 1984, Oceanic ridge volumes and sea level change – An error analysis, *in* Schlee, J., ed., Interregional unconformities and hydrocarbon accumulation: AAPG Memoir 36, p.109-127.

Kominz, M.A., Miller, K.G., and Browning, J.V., 1998, Long-term and short-term global Cenozoic sea-level estimates: Geology, v.26, n. 4, p.311-314.

Kominz, M.A., and Pekar, S.F., 2000, Oligocene eustasy from two-dimensional sequence stratigraphic backstripping: GSA Bulletin, *in* Press.

Magara, K., 1980, Comparison of porosity-depth relationships of shale and sandstone: J. Pet. Geol., 3, p.175-185.

McKenzie, D., 1978, Some remarks on the development of sedimentary basins: Earth and Planetary Science Letters, v.40, p.25-32.

Meade, R.H., 1964, Removal of water and rearrangement or particles during compaction of clayey sediments- A review: Geol. Surv. Prof. Pap., 497-B, 23 p.

Miller, K.G., 1997, Coastal Plain Drilling and the New Jersey Sea-Level Transect, *in* Miller, K.G., Snyder, S.W., et al., 1997, Proc. ODP, Sci. Results, 150 X, p. 3-12.

Miller , K.G., Mountain, G.S., the Leg 150 Shipboard Party, and Members of The New Jersey Coastal Plain Drilling Project, 1996, Drilling and Dating New Jersey Oligocene-Miocene Sequences: Ice Volume, Global Sea Level, and Exxon Records: Science, v.271, p.1092-1095.

Miller, K.G., Sugarman, P., Van Fossen, M., Liu, C., Browning, J.V., Queen, D., Aubry, M.P., Burckle, L.D., Goss, M., and Bukry, D., 1994, Island Beach site report, *in* Miller, K.G., et al., Proc. ODP, Initial Reports, v.150X, p.5-33.

Miller, K.G., Sugarman, P.G., Browning, J.V., Olsson, R.K., Pekar, S.F., Reilly, T.J., Cramer, B.S., Aubry, M.P., Lawrence, R.P., Curran, J., Stewart, M., Metzger, J.M., Uptegrove, J., Bukry, D., Burckle, L.H., Wright, J.D., Feigenson, M.D., Brenner, G.J., and Dalton, R.F., 1998, Bass River Site, *in* Miller, K.G., Sugarman, P.J., Browning, J.V., et al., Proc. ODP, Init. Repts., v. 174 AX, p.5-43.

Miller, K.G., Sugarman, P.J., Browning, J.V., Cramer, B.S., Olsson, R.K., de Romero, L., Aubry, M.P., Pekar, S.F., Georgescu, M.D., Metzger, K.T., Monteverde, D.H., Skinner, E.S., Uptegrove, J., Mullikin, L.G., Muller, F.L., Feigenson, M.D., Reilly, T.J., Brenner, G.J., and Queen, D., 1999, Ancora Site, *in* Miller, K.G., Sugarman, P.J., Browning, J.V., et al., Proc. ODP, Init. Repts., 174 AX (Suppl.), Available from World Wide Web: <http://www-odp.tamu.edu/publications/174AXSIR/VOLUME/CHAPTERS/174AXS_1.PDF>.

Nobes, D.C., Langseth, M.G., Kuramoto, S., and Holler, P., 1992, Identification and correction of a systematic error in index property measurements, *in* Tamaki, K., Suyehiro, K., Allan, J., McWilliams, M., et al., Proc. ODP, Sci. Results, v.127/128, p.985-1015.

Olsson, R.K., Gibson, T.G., Hansen, H.J., and Owens, J.P., 1988, Geology of the northern Atlantic coastal plain: Long Island to Virginia, *in* Sheridan, R.E., and Grow, J.A., eds., The Atlantic Continental Margin, U.S.: Boulder, Colorado, Geological Society of America, Geology of North America, v.1-2, p.87-105.

Owens, J.P., and Gohn, G.S., 1985, Depositional History of the Cretaceous series in the U.S. coastal plain: Stratigraphy, paleoenvironments, and tectonic controls of sedimentation, *in* Poag, L.W., ed., Geologic evolution of the United States Atlantic margin: Van Nostrand Reinhold, New York, p.25-86.

Owens, J.P., and Sohl, N., 1969, Shelf and deltaic paleoenvironments in the Cretaceous-Tertiary formations of the New Jersey Coastal Plain, *in* Subitsky, S., ed., Geology of selected areas in New Jersey and eastern Pennsylvania and guidebook of excursions: Rutgers University Press, New Brunswick, N.J., p.235-278.

Owens, J.P., Sugarman, P.J., Sohl, N.F., Parker, R.A., Houghton, H.F., Volkert, R.A., Drake, A.A., and Orndorff, R.C., 1998, Bedrock geologic map of Central and southern New Jersey: USGS Misc. Investigations Series Map I-2540-B.

Poag, C.W., 1992, U.S. middle Atlantic continental rise: provenance, dispersal, and deposition of Jurassic to Quaternary sediments, in Poag, C.W., and de Graciansky, P.C., eds., Geologic evolution of Atlantic continental rises: New York, Van Nostrand, p.100-156.

Poag, C.W., and Sevon, W.D., 1989, A record of Appalachian denudation in postrift Mesozoic and Cenozoic sedimentary deposits of the U.S. middle Atlantic continental margin: Geomorphology, v.2, p.119-157.

Posamentier, H.W., Jervey, M.T., and Vail, P.R., 1988, Eustatic controls on clastic deposition II – conceptual framework, *in* Wilgus, C.K., Hastings, C.K., St. Kendall, C.G., Posamentier, H.W., Ross, C.A., and Van Wagoner, J.C., Sea-level changes: An integrated approach, SEPM Special Publication 42, p.125-154.

Rhodehamel, E.C., 1977, Sandstone porosities, *in* Scholle, P.A., ed., Geological studies on the COST No. B-2 well, U.S. mid-Atlantic outer continental shelf area: U.S. Geological Survey Circular 750, p.23-31.

Schlumberger, 1972, Log interpretation/ charts: Houston, Texas, Schlumberger Well Services, Inc.

Schlumberger, 1974, Log interpretation - applications: New York, Schlumberger Limited, v.2, 116 p.

Sleep, N.H., 1971, Thermal effects of the formation of Atlantic continental margins by continental breakup: Royal Astronomical Society Geophysical Journal, v.24, p.325-350.

Steckler,M.S., and Watts, A.B., 1978, Subsidence of the Atlantic-type continental margins off New York: Earth and Planetary Science Letters, v. 41, p.1-13.

Steckler, M.S., Watts, A.B., and Thorne, J.A., 1988, Subsidence and basin modeling at the U.S. Atlantic passive margin, *in* Sheridan, R.E., and Grow, J.A., eds., The Atlantic Continental Margin, U.S.: Boulder, Colorado, Geological Society of America, Geology of North America, v.1-2, p.399-416.

Steckler,M.S., Mountain, G.S., Miller, K.G., and Christie-Blick, N., 1999, Reconstruction of Tertiary progradation and clinoform development on the New Jersey passive margin by 2-D backstripping: Marine Geology, v.154, p.399-420.

Stein, C.A., and Stein, S., 1992, A model for the global variation in oceanic depth and heat flow with lithospheric age: Nature, v.359, p.123-129.

Stoll, R.D., 1989, Sediment Acoustics, Springer-Verlag, New York, 153 p.

Vail, P.R., 1988, Seismic stratigraphy interpretation using sequence stratigraphy, Pt. 1: Seismic stratigraphy interpretation procedure, *in* Bally, A.W., ed., Atlas of seismic stratigraphy: Techniques papers and method oriented papers: AAPG Studies in Geology, n.27, v.1, p.1-10.

Velde, B., 1996, Compaction trends of clay-rich deep sea sediments: Marine Geology, v.133, p.193-201.

Watts, A.B., 1981, The U.S. Atlantic continental margin; Subsidence history, crustal structure, and thermal evolution, *in* Bally, A.W., ed., Geology of passive continental margins; History, structure, and sedimentologic record: AAPG Education Course Note Series, n.19, p.2-i-2 – 70.

Wyllie, M.R.J., Gregory, A.R., and Gardner, G.H.F., 1958, An experimental investigation of the factors affecting elastic wave velocities in porous media: Geophysics, v.23, p.459-493.